→ 3rd ADVANCED COURSE ON RADAR POLARIMETRY

Polarimetric SAR Tomography

Advanced Concepts

Laurent Ferro-Famil, University of Rennes 1
Stefano Tebaldini, Politecnico di Milano

19–23 January 2015 | ESA-ESRIN | Frascati (Rome), Italy

European Space Agency

Scattering Mechanism Decomposition

Decompose the data covariance matrix into ground-only and volume-only contributions

$$\mathbf{y} = \begin{bmatrix} \mathbf{y}_{MB}(\mathbf{w}_1) \\ \mathbf{y}_{MB}(\mathbf{w}_2) \\ \mathbf{y}_{MB}(\mathbf{w}_3) \end{bmatrix}$$

$$\mathbf{W} = E[\mathbf{y}\mathbf{y}^H] = \mathbf{W}_g + \mathbf{W}_v$$

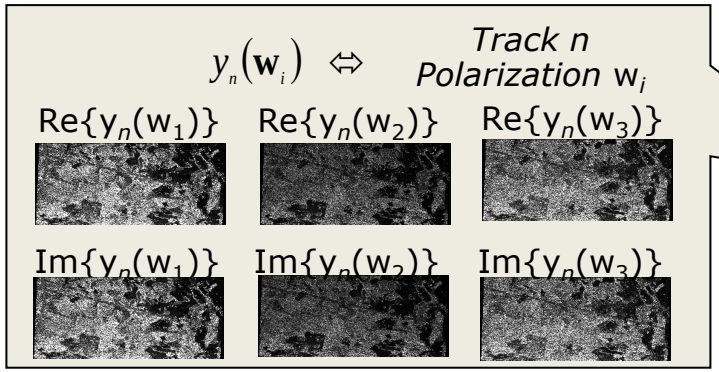

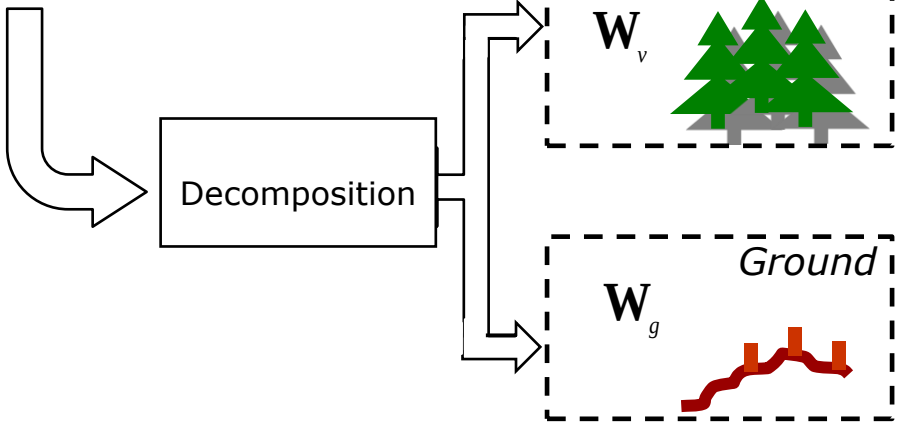

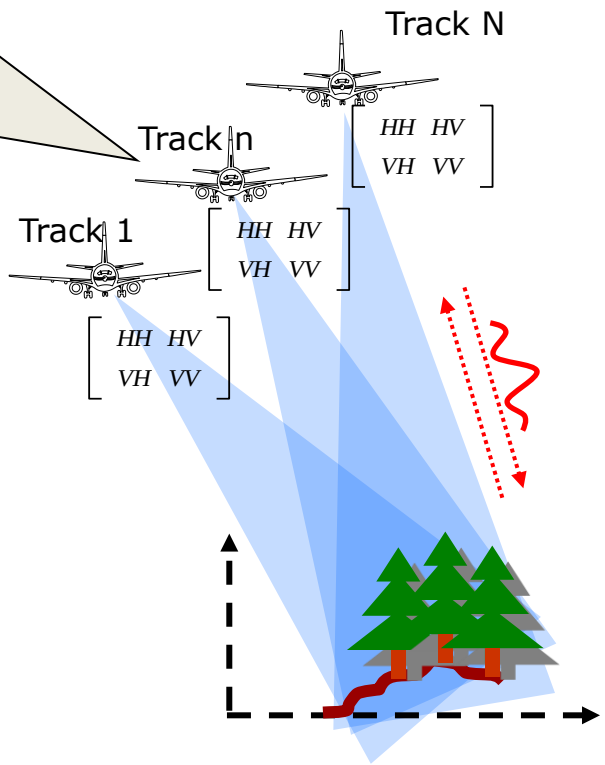

Scattering Mechanism Decomposition

Ground-volume decomposition implies:

- Separation of Structural Properties

=> Separated Tomographic Imaging of Ground-only and Volume-only Contributions

HV

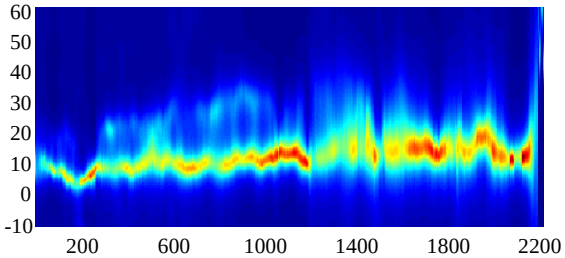

Ground

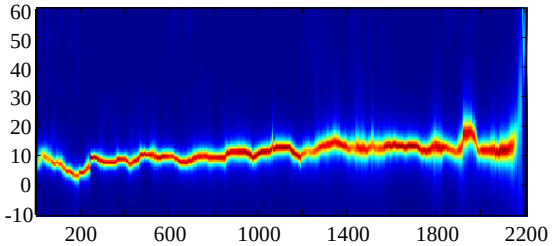

Volume

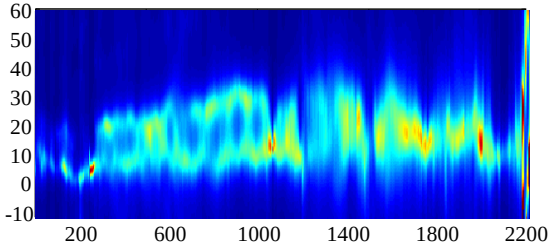

- Separation of Polarimetric Properties

=> Evaluation of the Ground to Volume Backscattered Power Ratio for each polarization

P-Band HH

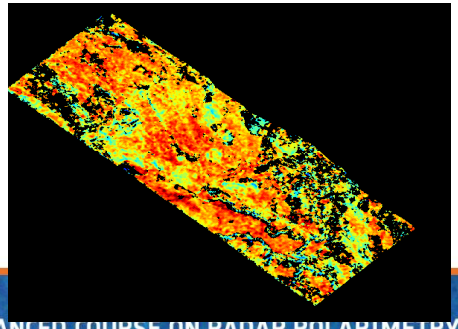

P-Band HV

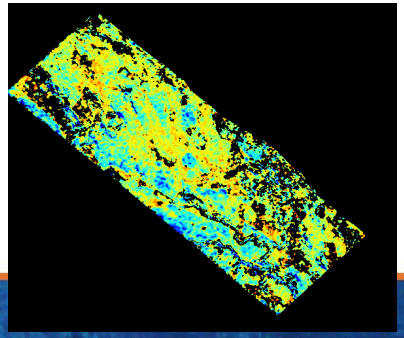

L-Band HH

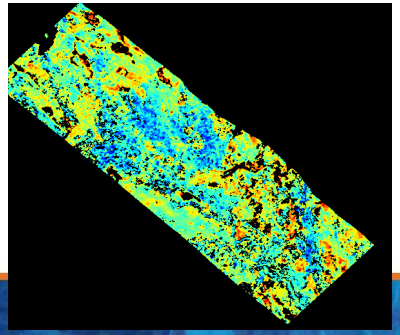

L-Band HV

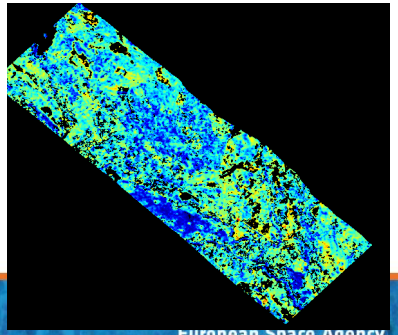

Radar scattering from forested areas

Forested areas are usually modeled in literature as the ensemble of trunks, terrain, and canopies, to be intended as a volume of random scatterers representing leaves and branches

The different kinds of interaction of the wave with such objects are referred to as ***Scattering Mechanisms*** (SMs)

Backscattering from the ground

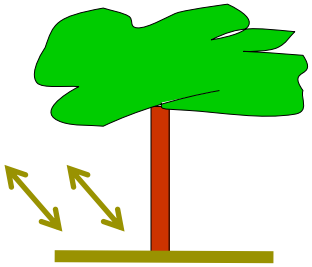

The wave is backscattered as a result of terrain roughness

Backscattering from the canopy:

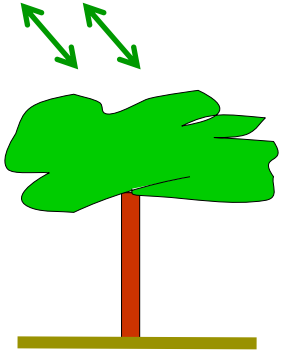

The wave is backscattered by the ensemble of braches and leaves that constitute the tree canopies

Ground-trunk double bounce scattering

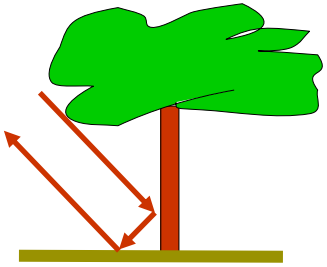

The wave is scattered in the specular direction and then reflected back to the SAR sensor

Radar scattering from forested areas
Tomographic (Interferometric) characterization

Each SM is associated with a different cross-range distribution ⇔ different InSAR coherence matrix

Coherence estimation (spatial multilooking)

$$\gamma_{nm} = \frac{\langle d_n d_m{}^* \rangle_L}{\sqrt{\langle |d_n|^2 \rangle_L \langle |d_m|^2 \rangle_L}} \Rightarrow \mathbf{R} = \begin{bmatrix} 1 & \gamma_{12} & \cdots & \gamma_{1N} \\ \gamma_{21} & 1 & & \\ \vdots & & \ddots & \vdots \\ \gamma_{N1} & & \cdots & 1 \end{bmatrix}$$

Coherence matrix (NxN)

Backscattering from the ground

The peak is ground locked

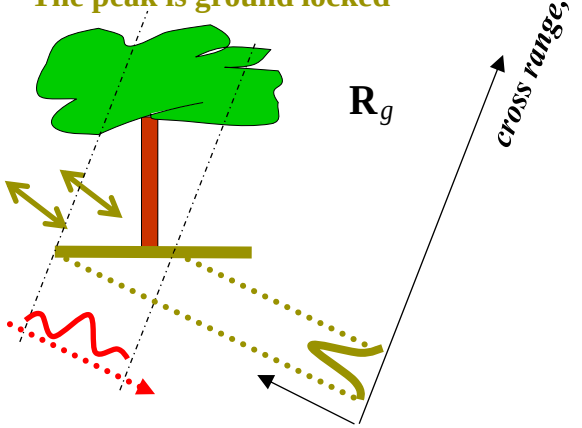

Backscattering from the canopy:

The peak is above the ground level

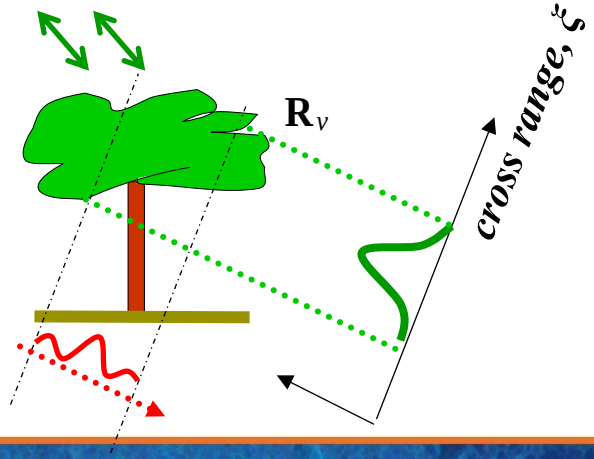

Ground-trunk double bounce scattering

The peak is ground locked

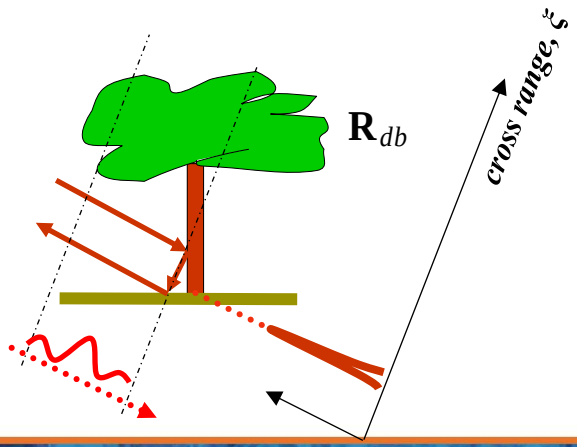

Each SM is associated with a different EM properties ⇔ different PolSAR covariance matrix

Coherence estimation (spatial multilooking)

Coherence matrix (3x3)

$$C_{nm} = \langle \boldsymbol{d}(\boldsymbol{w_1})\boldsymbol{d}^*(\boldsymbol{w_2})\rangle_L \Rightarrow \mathbf{C} = \begin{bmatrix} HHHH & HHHV & HHVV \\ HVHH & HVHV & HVVV \\ VVHH & VVHV & VVVV \end{bmatrix}$$

Backscattering from the ground

Ground Fresnel coefficients and roughness

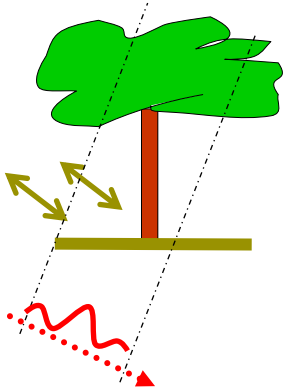

$\mathbf{C}_g$

$$C_g = s_g \begin{bmatrix} |\eta|^2 & 0 & \eta \\ 0 & 0 & 0 \\ \eta^* & 0 & 1 \end{bmatrix}$$

Backscattering from the canopy:

mean orientation of branches and leaves

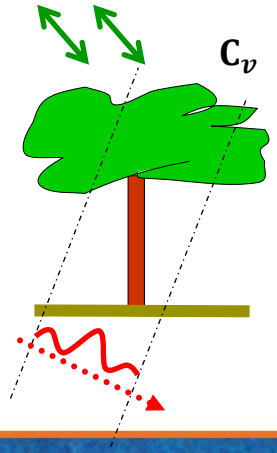

$\mathbf{C}_v$

$$C_v = s_v \begin{bmatrix} 1 & 0 & \rho \\ 0 & 1-\rho & 0 \\ \rho & 0 & 1 \end{bmatrix}$$

Ground-trunk double bounce scattering

Ground and trunk Fresnel coefficients and propagation through adjacent canopies

$\mathbf{C}_{db}$

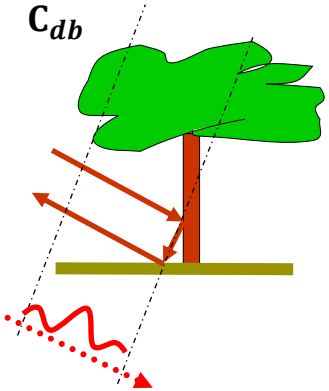

$$C_{db} = s_{db} \begin{bmatrix} |\alpha|^2 & 0 & \alpha \\ 0 & 0 & 0 \\ \alpha^* & 0 & 1 \end{bmatrix}$$

Three fundamental hypotheses will be retained:

H1): Statistical independence among different SMs

H2): Invariance of the interferometric coherences of each SM w.r.t. polarization

=> negligible variation of the EM properties of each SM (subsurface penetration, volume extinction,…) w.r.t. polarization

H3): Invariance of the polarimetric signature of each SM on the choice of the track

=> events like floods, fires, frosts, are expected not to occur during the acquisition campaign

Under such hypotheses the second order moments of the MPMB data are obtained as:

$$y_n(\mathbf{w}_i) = \sum_{k=1}^{K} s_k(n;\mathbf{w}_i) \xrightarrow{H1)\ H2)\ H3)} E[y_n(\mathbf{w}_i)y_m^*(\mathbf{w}_j)] = \sum_{k=1}^{K} c_k(\mathbf{w}_i,\mathbf{w}_j)\gamma_k(n,m)$$

- $c_k(\mathbf{w}_i,\mathbf{w}_j)$: polarimetric correlation of the *k-th* SM in Polarizations $\mathbf{w}_i, \mathbf{w}_j$

$$c_k(\mathbf{w}_i,\mathbf{w}_j) = E[s_k(n;\mathbf{w}_i)s_k^*(n;\mathbf{w}_j)]$$

- $\gamma_k(n,m)$: interferometric coherence of the *k-th* SM in the *nm-th* interferogram

$$\gamma_k(n,m) = \frac{E[s_k(n;\mathbf{w}_i)s_k^*(m;\mathbf{w}_j)]}{\sqrt{E\left[|s_k(n;\mathbf{w}_i)|^2\right]E\left[|s_k(m;\mathbf{w}_j)|^2\right]}}$$

Sum of Kronecker Products (SKP)

In vector notation H1), H2), H3) results in the data covariance matrix to be expressed as a Sum of Kronecker Products (SKP)

$$E[y_n(\mathbf{w}_i)y_m^*(\mathbf{w}_j)] = \sum_{k=1}^{K} c_k(\mathbf{w}_i,\mathbf{w}_j)\gamma_k(n,m) \quad \Leftrightarrow \quad \mathbf{W} = E\,[\mathbf{y}\mathbf{y}^H] = \sum_{k=1}^{K} \mathbf{C}_k \otimes \mathbf{R}_k$$

$$\mathbf{y} = \begin{bmatrix} y_1(\mathbf{w}_1) & \cdots & y_N(\mathbf{w}_1) & y_1(\mathbf{w}_2) & \cdots & y_N(\mathbf{w}_2) & y_1(\mathbf{w}_3) & \cdots & y_N(\mathbf{w}_3) \end{bmatrix}^T \qquad \{\mathbf{C}_k\}_{ij} = c_k(\mathbf{w}_i,\mathbf{w}_j) \qquad \{\mathbf{R}_k\}_{nm} = \gamma_k(n,m)$$

Each SM is represented by a Kronecker Product of two matrices:

Polarimetric Signature, $\mathbf{C}_k$:

polarimetric covariance matrix of the *k-th* SM alone [3 x 3]

⇔ Electromagnetic properties associated with the *k-th* SM

Structure Matrix, $\mathbf{R}_k$:

matrix of the interferometric coherences of the *k-th* SM alone [N x N]

⇔ Spatial structure of the backscattered power distribution associated with the *k-th* SM

Note that $\mathbf{R}_k$, $\mathbf{C}_k$ are (semi) positive definite matrices by definition

SKP Decomposition

The key to the exploitation of the SKP structure is existence of a technique (*) for the decomposition of *any* matrix into a SKP:

$$\mathbf{W} = \sum_{k=1}^{K} \lambda_k \widetilde{\mathbf{C}}_k \otimes \widetilde{\mathbf{R}}_k \qquad \lambda_1 \geq \lambda_2 \geq \ldots \geq 0$$

where $\left\{\widetilde{\mathbf{C}}_k\right\}$ **and** $\left\{\widetilde{\mathbf{R}}_k\right\}$ **are two sets of matrices obtained from W through an SVD-like analysis**

(*) Van Loan and Pitsianis, "Approximation with Kronecker products", Linear Algebra for Large Scale and Real Time Applications

Two major results follow:

***R1)* The best Least Square (LS) approximation of W with *K* KPs is obtained by retaining the first *K* terms of the SKP Decomposition of W (*Eckart-Young-Mirsky theorem*)**

⟹ **Lower Bound for *any* physical model that can be written as a sum of *K* KPs**

R2) **Given the data covariance matrix, *K* SMs are uniquely identified by *K*(*K-1*) real numbers** (***Algebraic Synthesis of Forest Scenarios from Multi-Baseline PolInSAR Data*** **– S. Tebaldini –TGRS, 2009)**

Corollary: **If only ground and volume scattering occurs:**

$$\mathbf{W} = \mathbf{C}_g \otimes \mathbf{R}_g + \mathbf{C}_v \otimes \mathbf{R}_v$$

then, there exist *two* real numbers a, b such that:

$$\mathbf{R}_g = a\widetilde{\mathbf{R}}_1 + (1-a)\widetilde{\mathbf{R}}_2 \qquad \mathbf{C}_g = \frac{1}{a-b}\left((1-b)\lambda_1\widetilde{\mathbf{C}}_1 - b\lambda_2\widetilde{\mathbf{C}}_2\right)$$

$$\mathbf{R}_v = b\widetilde{\mathbf{R}}_1 + (1-b)\widetilde{\mathbf{R}}_2 \qquad \mathbf{C}_v = \frac{1}{a-b}\left(-(1-a)\lambda_1\widetilde{\mathbf{C}}_1 + a\lambda_2\widetilde{\mathbf{C}}_2\right)$$

a **⇔ ground structure matrix $\mathbf{R}_g$ and volume polarimetric signature $\mathbf{C}_v$ (up to a scale factor)**

b **⇔ volume structure matrix $\mathbf{R}_v$ and ground polarimetric signature $\mathbf{C}_g$ (up to a scale factor)**

SKP Decomposition

General procedure for ground and volume decomposition

Approximate W by retaining the first two KPs of the SKP Decomposition

Choose the proper values of *a*, *b* :

1. **Select values of *a*, *b* that give rise to (semi) positive definite R_g, R_v, C_g, C_v**

   ⇔ physical validity of the solution

2. **Optimize some criterion in order to pick a unique solution**

SKP Decomposition

General procedure for ground and volume decomposition

Approximate W by retaining the first two KPs of the SKP Decomposition

Choose the proper values of *a*, *b* :

1. **Select values of *a*, *b* that give rise to (semi) positive definite R_g, R_v, C_g, C_v**

   ⇔ physical validity of the solution

2. **Optimize some criterion in order to pick a unique solution**

Region of physical validity for the ground and volume coherences in the interferometric pair formed between tracks 1 and 2 (Numerical simulation)

Coherence Locus – N = 2

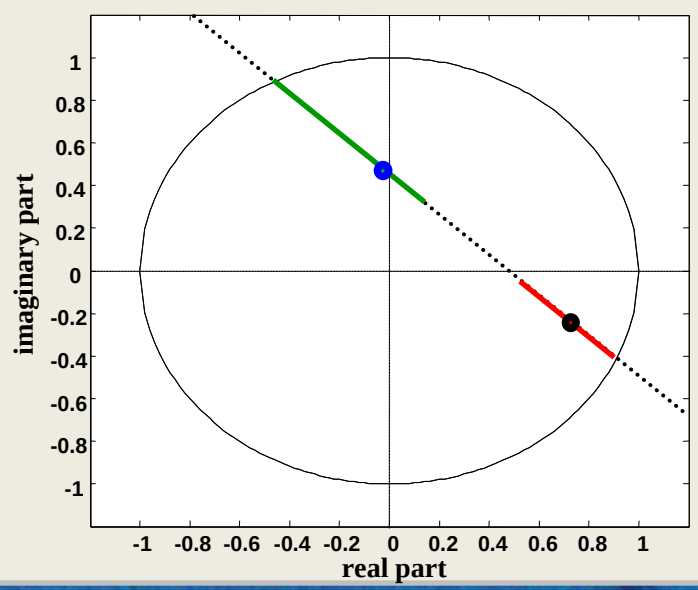

Single Baseline case :

The region of physical validity is formed by two branches, spanned by the parameters *a*, *b*

The union of branches *a*, *b* results in the same region of physical validity as in PolInSAR

Physically valid solutions

Branch a

Branch b

True Volume Coherence

True Ground Coherence

SKP Decomposition

General procedure for ground and volume decomposition

Approximate W by retaining the first two KPs of the SKP Decomposition

Choose the proper values of *a*, *b* :

1. **Select values of *a*, *b* that give rise to (semi) positive definite R_g, R_v, C_g, C_v**

   ⇔ physical validity of the solution

2. **Optimize some criterion in order to pick a unique solution**

Region of physical validity for the ground and volume coherences in the interferometric pair formed between tracks 1 and 2 (Numerical simulation)

Coherence Locus – N = 3

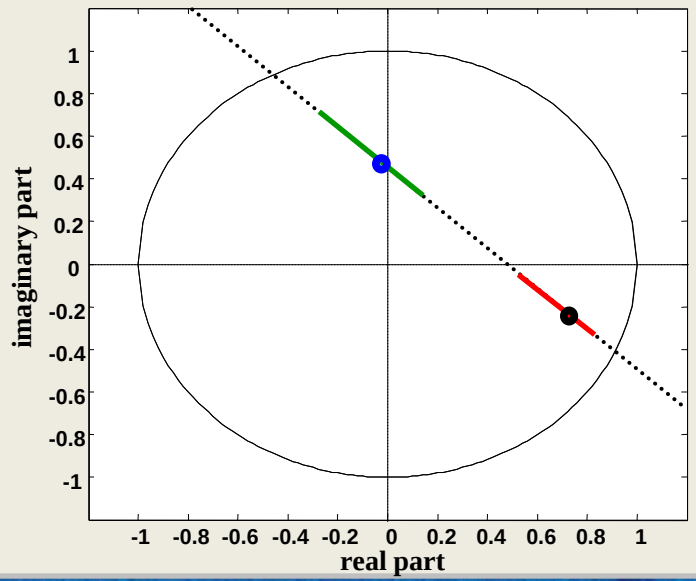

Multi-Baseline case : the region of physical validity tends to *shrink*, depending on the number of available tracks

Physically valid solutions

Branch a

Branch b

True Volume Coherence

True Ground Coherence

SKP Decomposition

General procedure for ground and volume decomposition

Approximate W by retaining the first two KPs of the SKP Decomposition

Choose the proper values of *a*, *b* :

1. **Select values of *a*, *b* that give rise to (semi) positive definite R_g, R_v, C_g, C_v**

   ⇔ physical validity of the solution

2. **Optimize some criterion in order to pick a unique solution**

Region of physical validity for the ground and volume coherences in the interferometric pair formed between tracks 1 and 2 (Numerical simulation)

Coherence Locus – N = 10

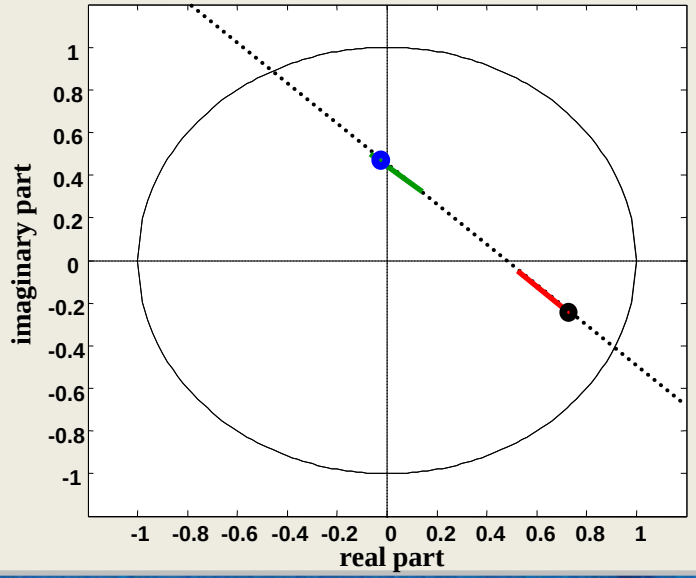

Multi-Baseline case : the region of physical validity tends to *shrink*, depending on the number of available tracks

- **The higher the number of tracks, the easier it is to pick the correct solution**

Physically valid solutions

Branch a

Branch b

True Volume Coherence

True Ground Coherence

SKP Decomposition

General procedure for ground and volume decomposition

Approximate W by retaining the first two KPs of the SKP Decomposition

Choose the proper values of *a*, *b* :

1. **Select values of *a*, *b* that give rise to (semi) positive definite R_g, R_v, C_g, C_v**
   ⇔ physical validity of the solution
2. **Optimize some criterion in order to pick a unique solution**

Despite the availability of multiple baselines, the problem of SM separation is always affected by an ambiguity, corresponding to the extent of the region of physical validity

All solutions in this region are physically valid and give rise to exactly the same data covariance matrix

⟹ **there is no way to assess algebraically which solution is correct**

It is then important to characterize each solution from a physical point of view, in order to

- **provide a correct interpretation of the results**
- **drive the choice of the criteria to be optimized at step 2**

Choice of the solution: physical interpretation

Simulated scenario

Presence of ground decorrelation

HV Ground Contributions

Simulated Backscattered Power Distributions

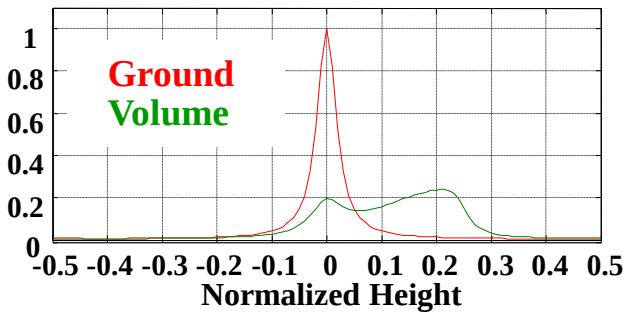

Simulated Polarimetric Signatures

$$\mathbf{C}_g = \begin{bmatrix} 1 & 0 & 0.8 \\ 0 & 0.1 & 0 \\ 0.8 & 0 & 1 \end{bmatrix} \qquad \mathbf{C}_v = \begin{bmatrix} 1 & 0 & 0.4 \\ 0 & 0.6 & 0 \\ 0.4 & 0 & 1 \end{bmatrix}$$

Two opposite solutions for each branch will be considered:

Outer Boundaries

Coherence Locus

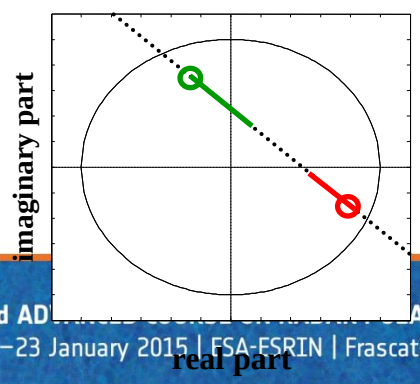

Inner Boundaries

Coherence Locus

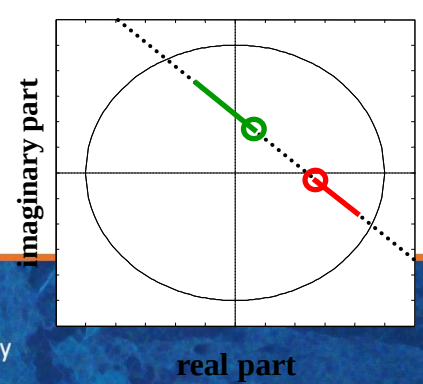

Note:

With no loss of generality, we will assume that branch *a* is associated with ground coherence and branch *b* with volume coherence

Solutions on branch *a*

Branch *a* ⇔ ground structure matrix R_g and volume polarimetric signature C_v

Outer Boundary Solution

Coherence Locus

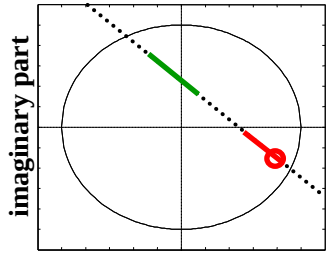

C_v is full rank – consistent with physical models for forest scattering

R_g is maximally coherent

The effective phase center is under-estimated for small *N* in presence of coherence losses

The resulting ground backscattered power distribution converges to the true one for large *N*, despite the presence of ground coherence losses

Resulting Backscattered Power Distribution

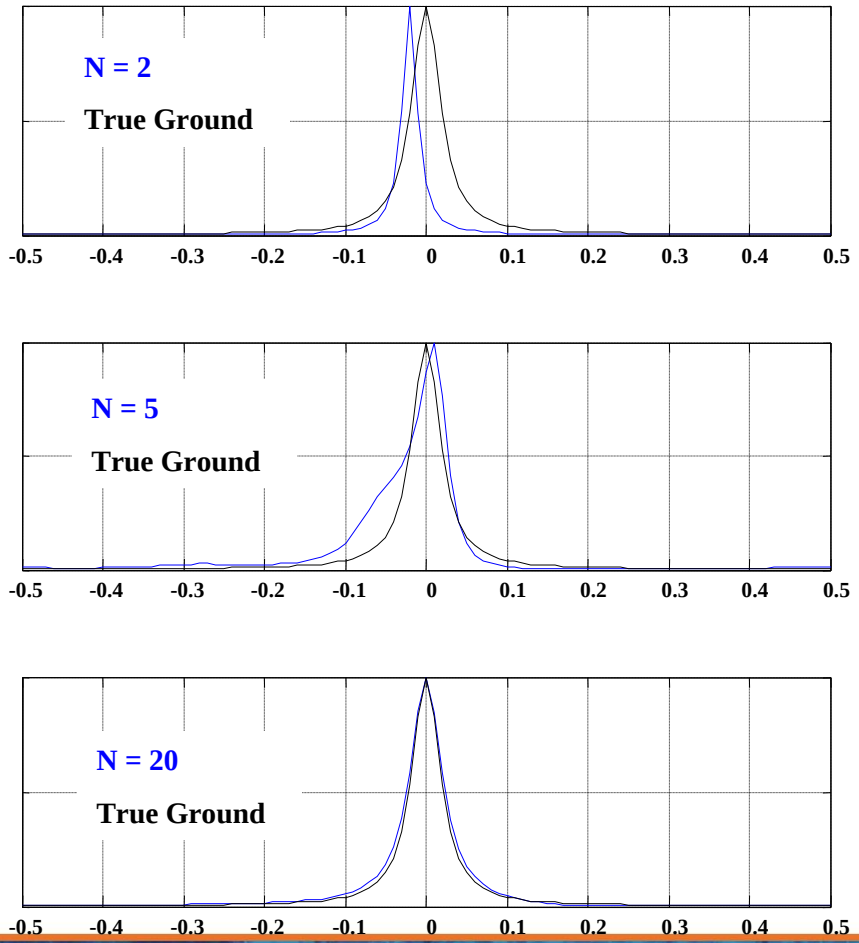

Solutions on branch *a*

Branch *a* ⇔ ground structure matrix R_g and volume polarimetric signature C_v

Inner Boundary Solution

Coherence Locus

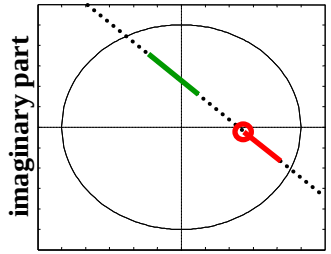

C_v is rank deficient – NOT consistent with physical models for forest scattering

R_g is less coherent than in the OB solution

For every *N*, the estimate is contaminated by volume contributions, resulting in apparent components from above the ground

Resulting Backscattered Power Distribution

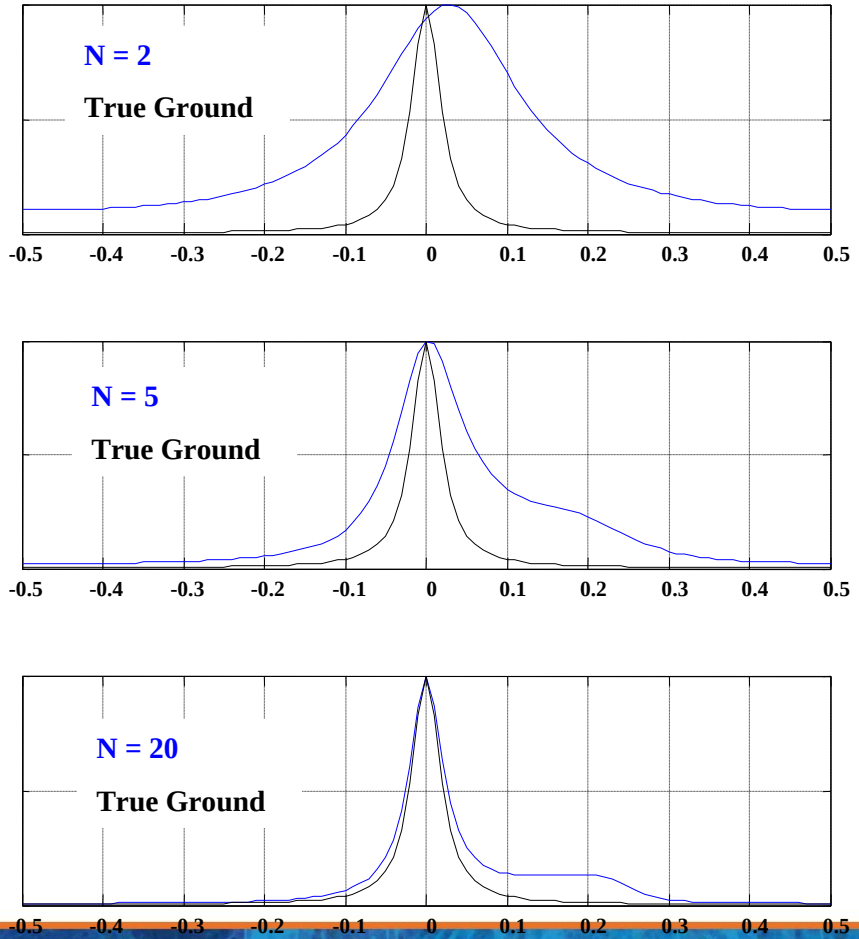

Branch *b* ⇔ volume structure matrix R_v and ground polarimetric signature C_g

Outer Boundary Solution

Coherence Locus

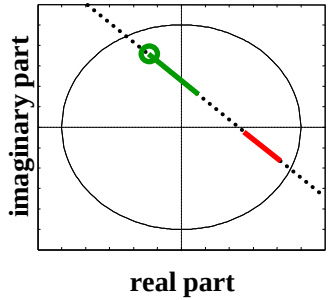

C_g is full rank – consistent with HV ground contributions

R_v is maximally coherent

For small *N*, the OB solution acts as a high-pass filter, resulting in the volume to appear thinner than it is

Asymptotical convergence to true structure of volume contributions above the ground, ground-level volume contributions being absorbed into ground structure

Resulting Backscattered Power Distribution

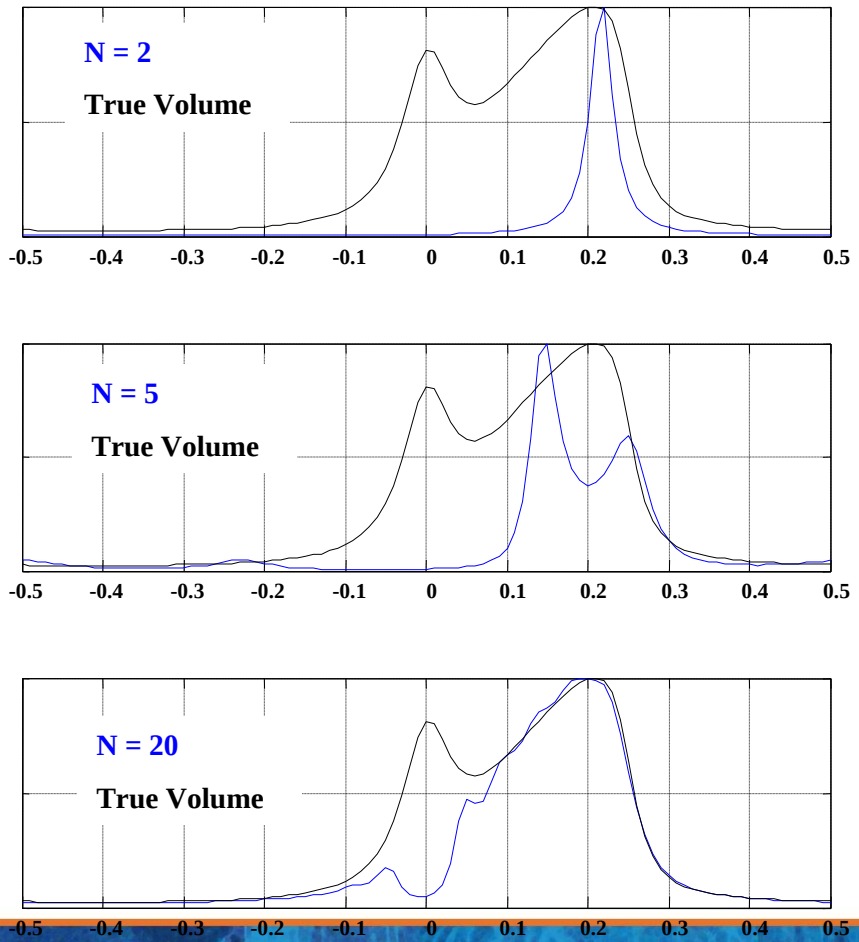

Solutions on branch *b*

Branch *b* ⇔ volume structure matrix R_v and ground polarimetric signature C_g

Inner Boundary Solution

Coherence Locus

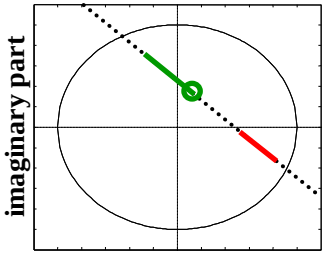

Resulting Backscattered Power Distribution

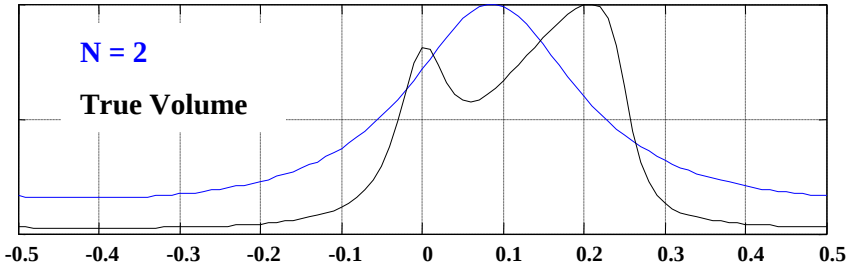

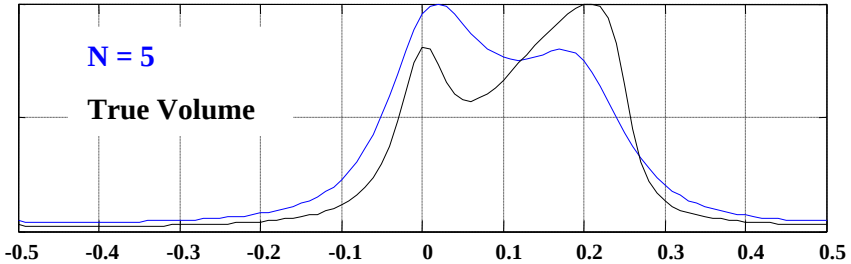

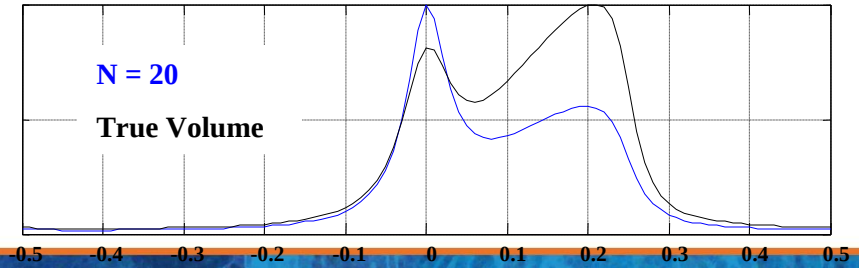

Normalized Height

R_v is less coherent than in the OB solution

C_g is rank deficient ⇔ there exists one polarization where volume only contributions are present

If this is not true, the resulting volume backscattered power distribution does not converge to the true one, as it is contaminated by ground contributions

Still, this is NOT a problem as for the determination of volume top height

To sum up:

Inner Boundary solution:

Provides the true solution for volume scattering if there exists one polarization unaffected by ground contributions

The resulting SMs are characterized by a full-rank and a rank-deficient polarimetric covariance matrix, therefore yielding a *Polarimetric* representation of the forest structure

Outer Boundary solution:

Converges to the true solution for volume scattering *above* the ground

The resulting SMs are associated with contributions from ground and canopy *levels*, therefore yielding a *Tomographic* representation of the forest structure

Volume top height is substantially invariant to the choice of the solution, therefore constituting the most robust indicator of the volume structure

Boundary Solutions

By definition, the points at the outer or inner boundaries of the two branches correspond to the case where one of the four matrices $\mathbf{C}_g$, $\mathbf{C}_v$, $\mathbf{R}_g$, $\mathbf{R}_v$ is singular

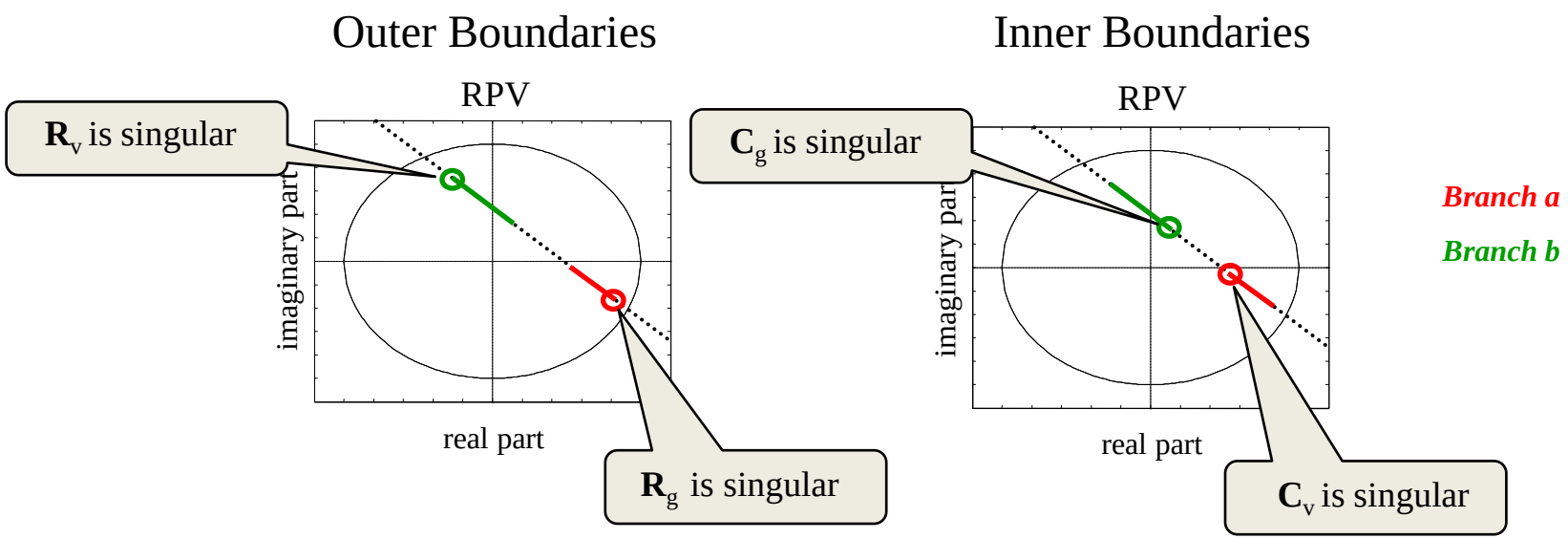

Branch *a* ⇔ **ground** structure matrix $\mathbf{R}_g$ and **volume** polarimetric signature $\mathbf{C}_v$

Branch *b* ⇔ **volume** structure matrix $\mathbf{R}_v$ and **ground** polarimetric signature $\mathbf{C}_g$

Each of the boundary solutions has a specific physical interpretation

Case Studies

Campaign	BioSAR 2007 - ESA
System	E-SAR - DLR
Period	Spring 2007
Site	Remningstorp, South Sweden
Scene	Semi-boreal forest
Topography	Flat
Tomographic tracks	9 – Fully Polarimetric
Carrier frequency	350 MHz
Slant range resolution	2 m
Azimuth resolution	1.6 m
Vertical resolution	10 m (near range) to 40 m (far range)

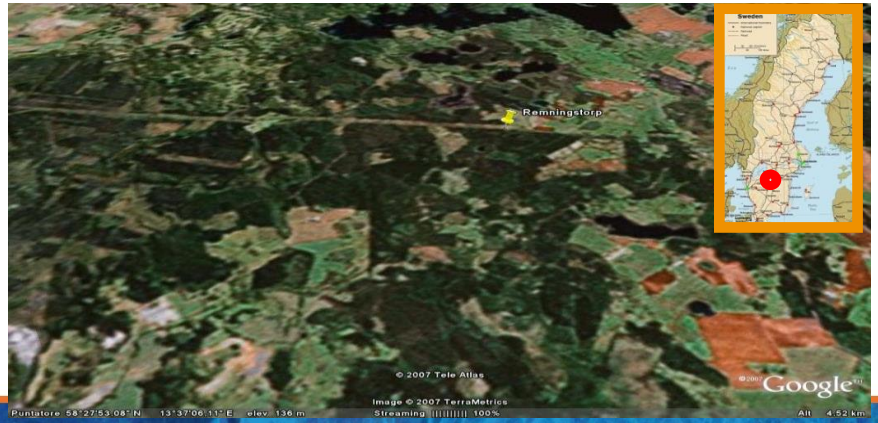

Case Studies

Tomographic reconstruction of an azimuth cut:

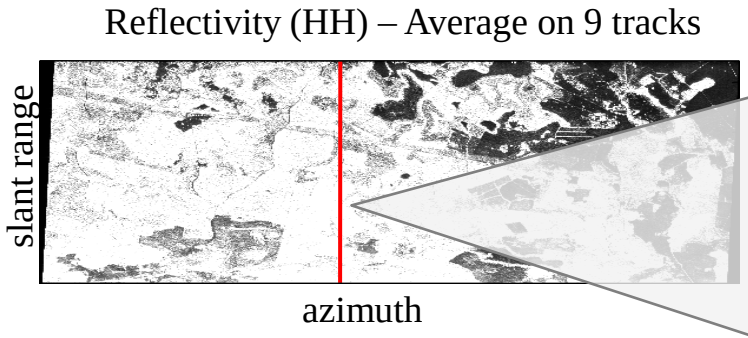

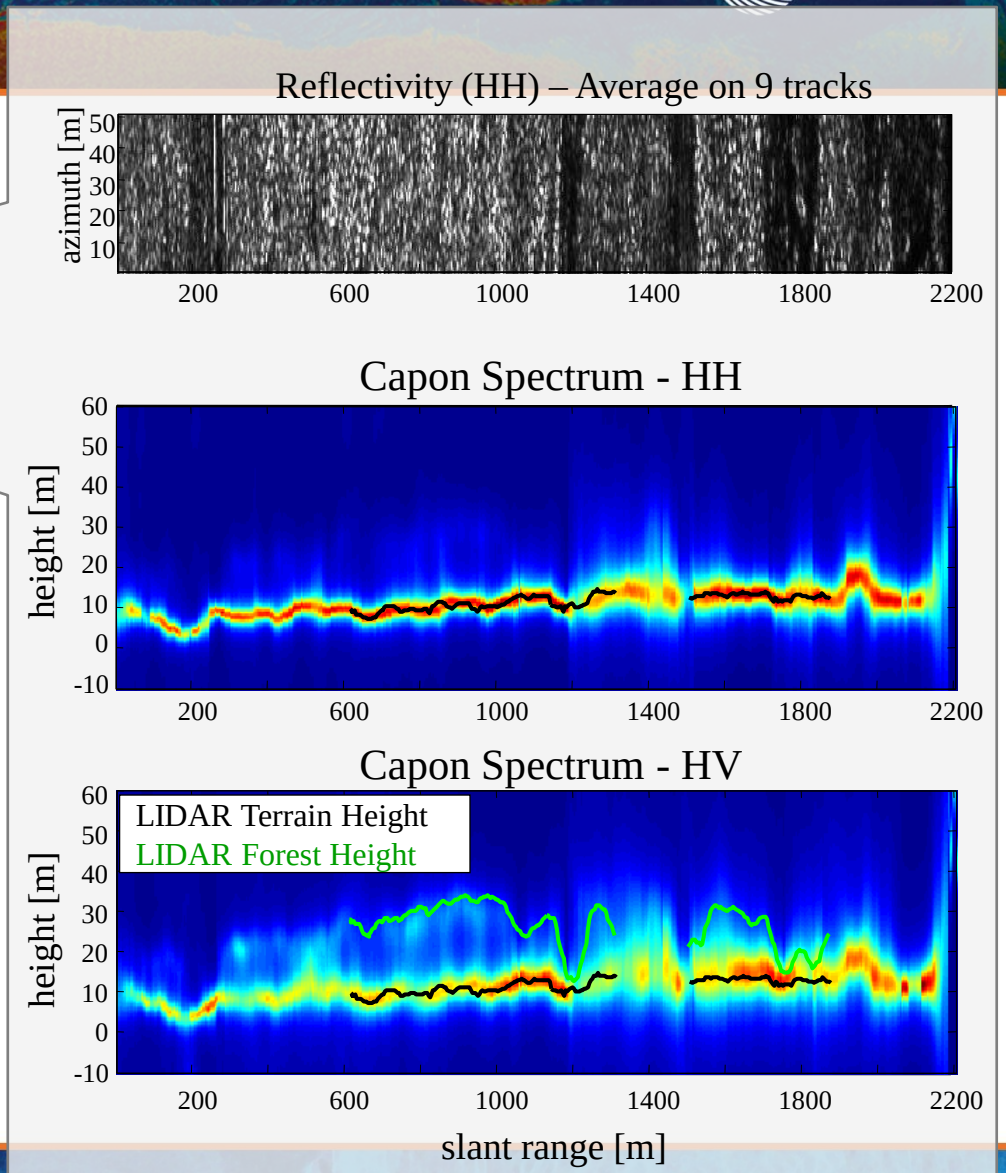

The analyzed profile is almost totally forested, except for the dark areas

HH:

Dominant phase center is ground locked
Vegetation is barely visible

Similar conclusions for VV

HV:

Dominant phase center is ground locked
Vegetation is much more visible

Case Studies

Model validation: $\mathbf{W} \overset{?}{=} \mathbf{C}_g \otimes \mathbf{R}_g + \mathbf{C}_v \otimes \mathbf{R}_v$

Methodology:

evaluation of the error between the sample covariance matrix and its best L2 approximation with $K = \{1,2,3,4\}$ KPs

$$\hat{\mathbf{W}}_K = \arg\min_{\mathbf{W}_k} \left\{ \left\| \hat{\mathbf{W}} - \mathbf{W}_K \right\|_F \right\}$$

$$error = \frac{\left\| \hat{\mathbf{W}} - \mathbf{W}_K \right\|_F}{\left\| \hat{\mathbf{W}} \right\|_F}$$

Remark: the best L2 approximation is obtained simply by taking the dominant K terms of the SKP decomposition

$$\left\| \hat{\mathbf{W}} - \hat{\mathbf{W}}_2 \right\|_F < 0.1 \cdot \left\| \hat{\mathbf{W}} \right\|_F$$

> 90 % of the information can be represented by the sum of just two KPs

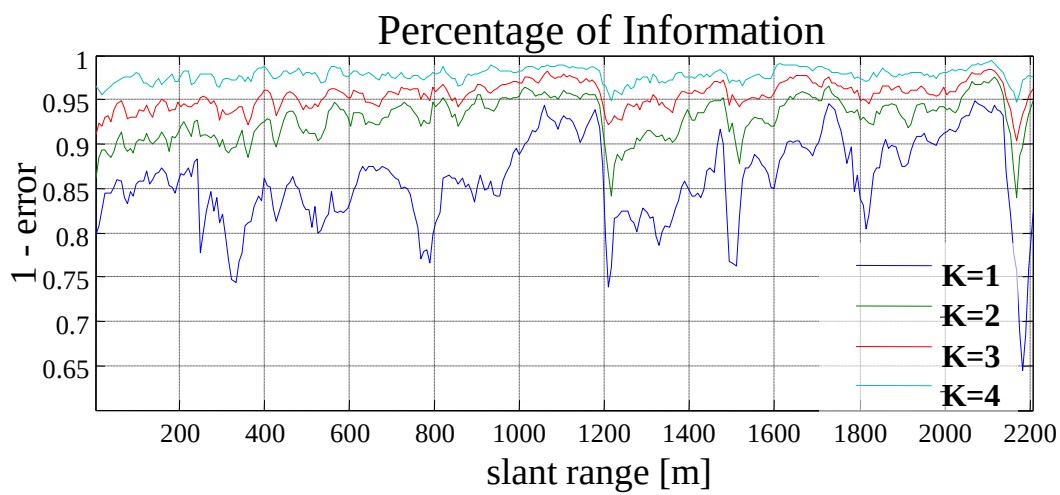

Inner boundary solutions

RPV

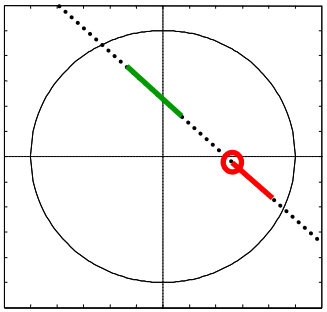

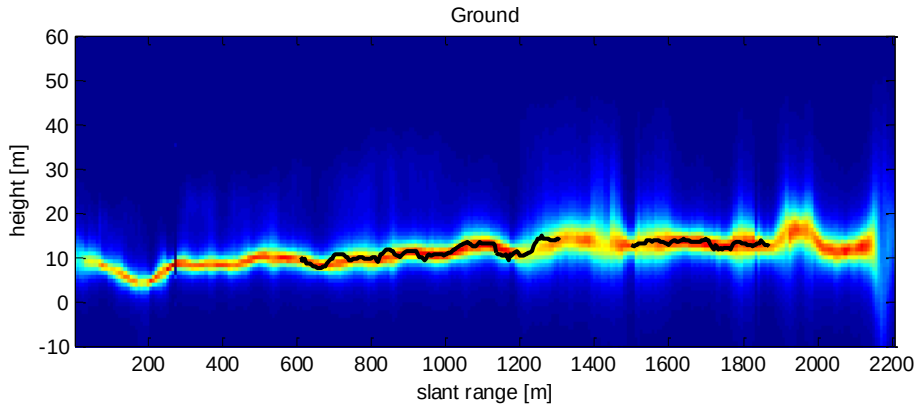

Residual volume contributions visible above the ground

Significant contributions from the ground level.
⇔ Volumetric scattering at the ground level
Consistent with:

- Backscattering from understorey or lower tree branches
- Multiple interactions of volumetric scatterers with the ground

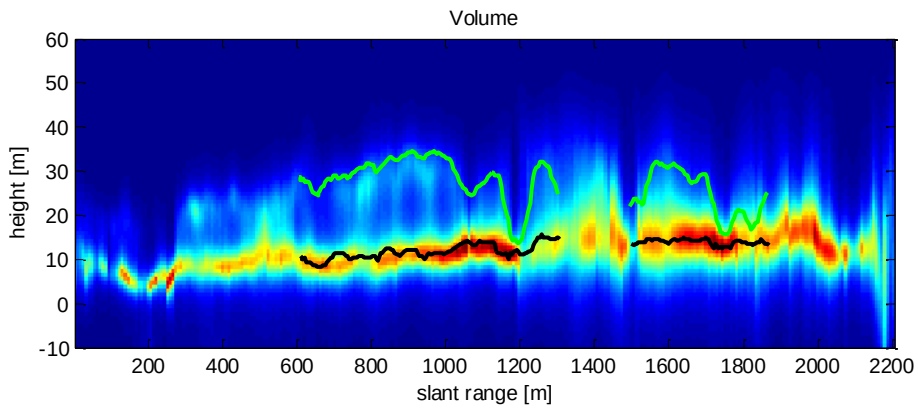

RPV

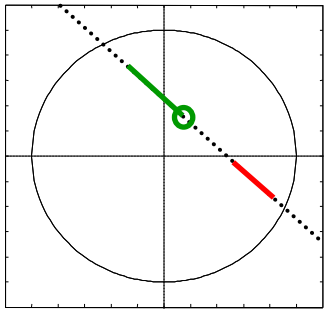

LIDAR Terrain Height
LIDAR Forest Height

Intermediate solutions

RPV

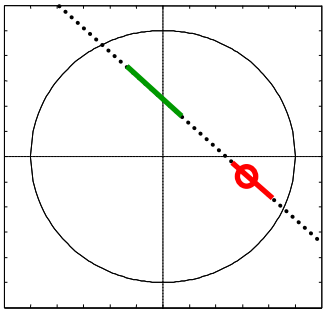

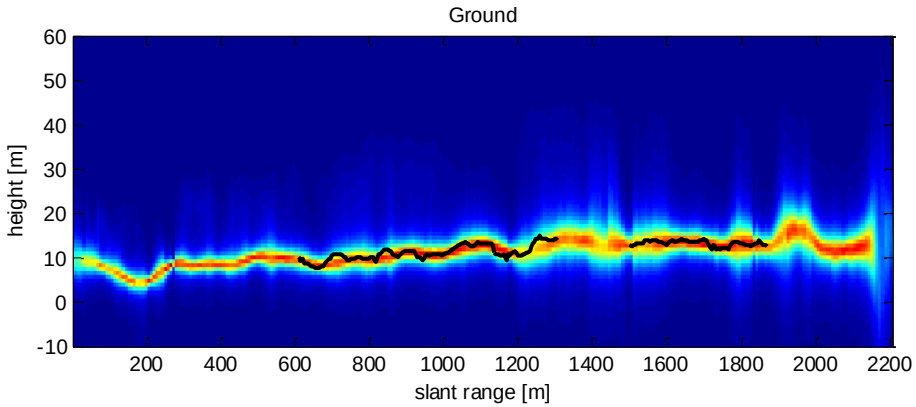

Improved volume rejection

Volumetric contributions from the ground level are partly rejected

Backscattering contributions from the whole volume structure are emphasized

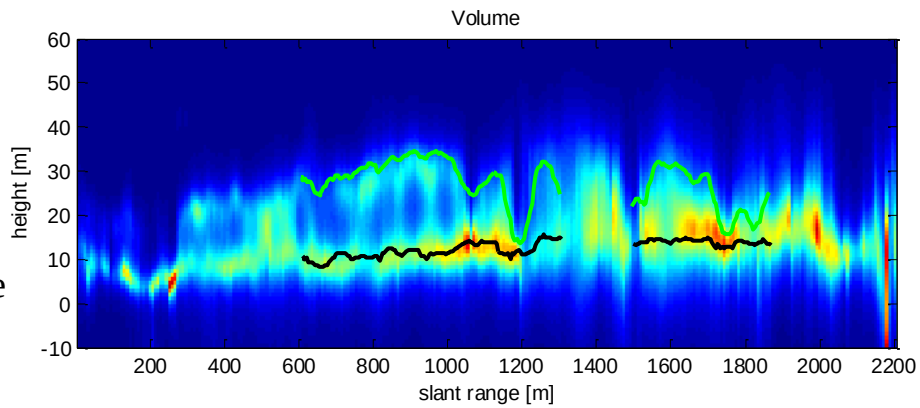

RPV

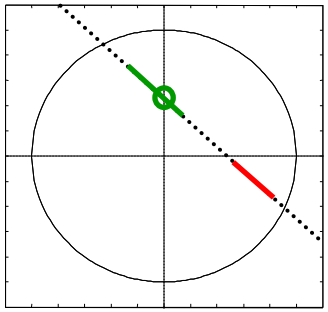

LIDAR Terrain Height
LIDAR Forest Height

Intermediate solutions

RPV

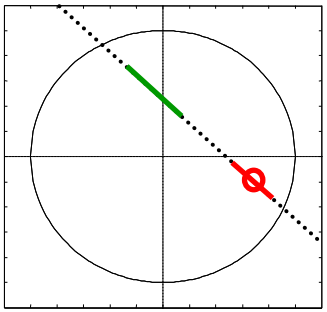

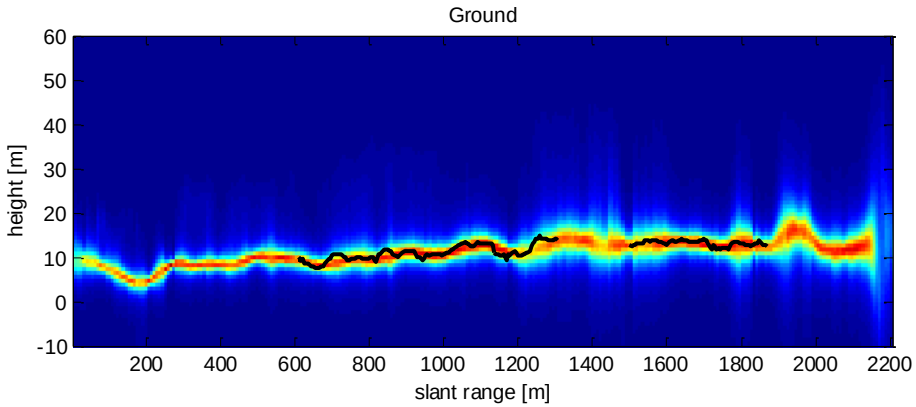

Improved volume rejection

Improved ground rejection

Backscattering contributions from the whole volume structure are emphasized

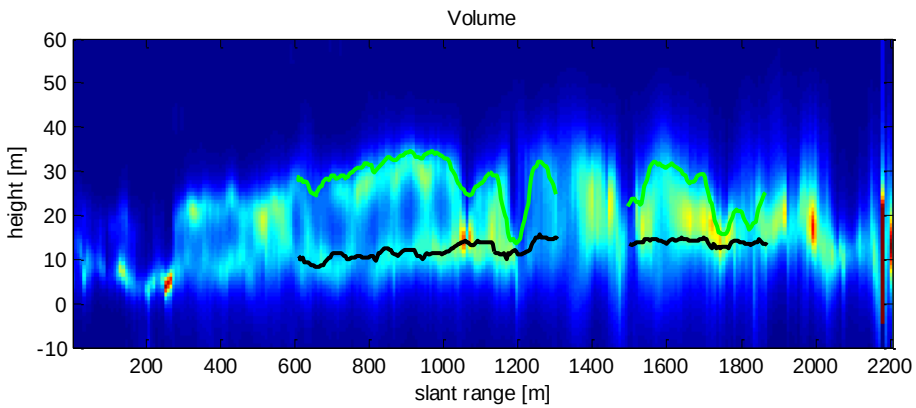

RPV

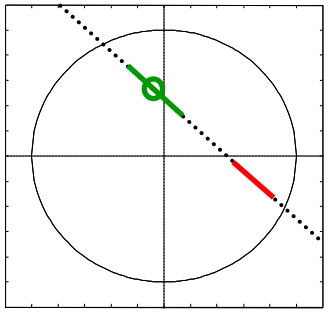

LIDAR Terrain Height
LIDAR Forest Height

Intermediate solutions

RPV

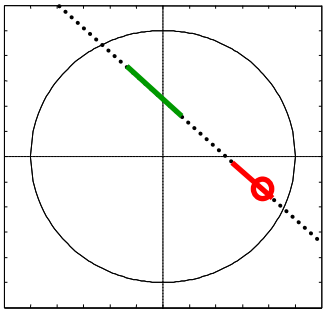

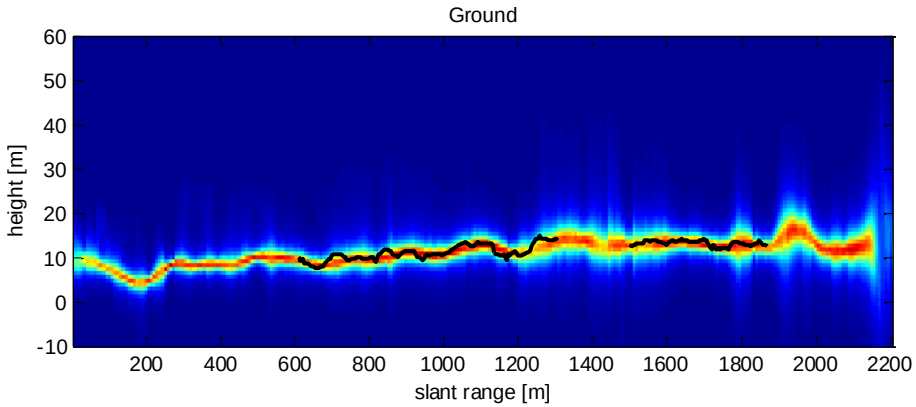

Improved volume rejection

Ground contributions rejected

Contributions from the lower canopy are partly rejected

Backscattering contributions from the upper volume structure are emphasized

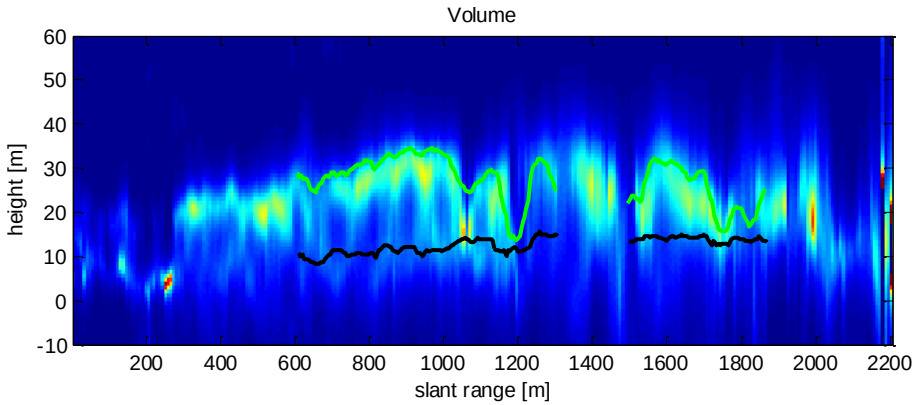

RPV

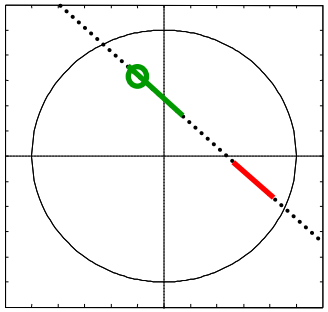

LIDAR Terrain Height
LIDAR Forest Height

Outer boundary solutions

RPV

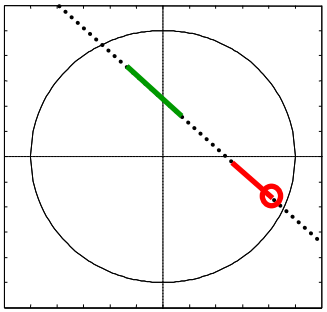

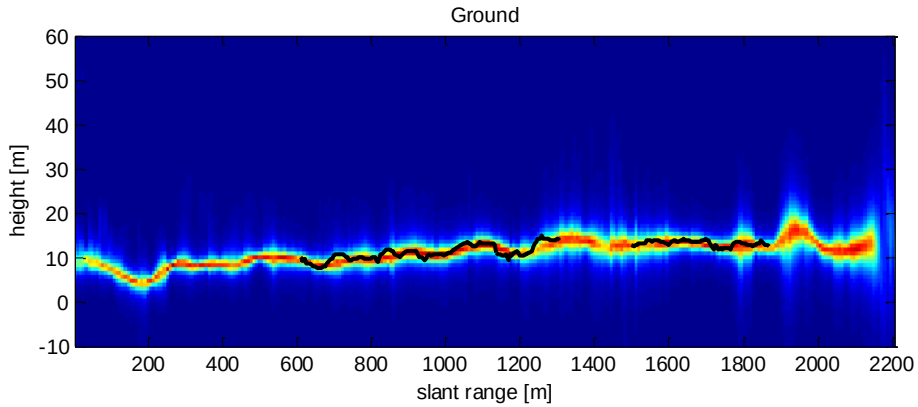

Maximum volume rejection

Ground structure is maximally coherent

Ground and lower canopy contributions are rejected

Only upper canopy contributions are visible

Volume structure is maximally coherent

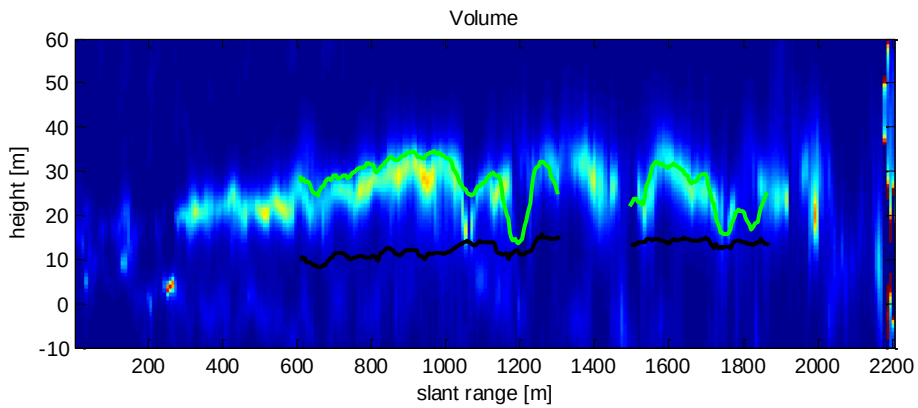

RPV

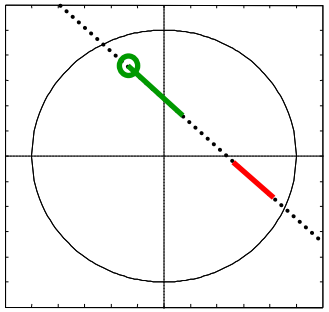

Volume top height is nearly invariant to the choice of the solution, therefore constituting a robust indicator of the volume structure

LIDAR Terrain Height
LIDAR Forest Height

Campaign	BioSAR 2008 - ESA
System	E-SAR - DLR
Site	Krycklan river catchment, Northern Sweden
Scene	Boreal forest
Topography	Hilly
Tomographic Tracks	6 + 6 – Fully Polarimetric (South-West and North-East)
Carrier Frequency	P-Band and L-Band
Slant range resolution	1.5 m
Azimuth resolution	1.6 m
Vertical resolution (P-Band)	20 m (near range) to >80 m (far range)
Vertical resolution (L-Band)	6 m (near range) to 25 m (far range)

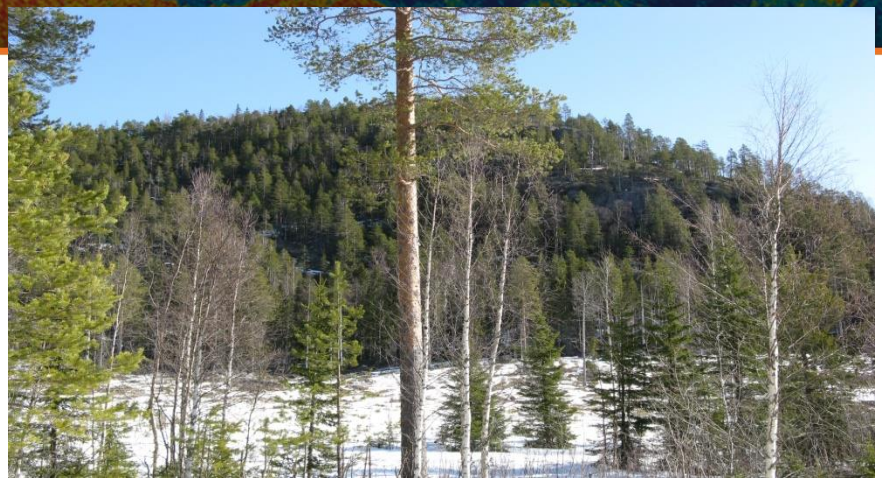

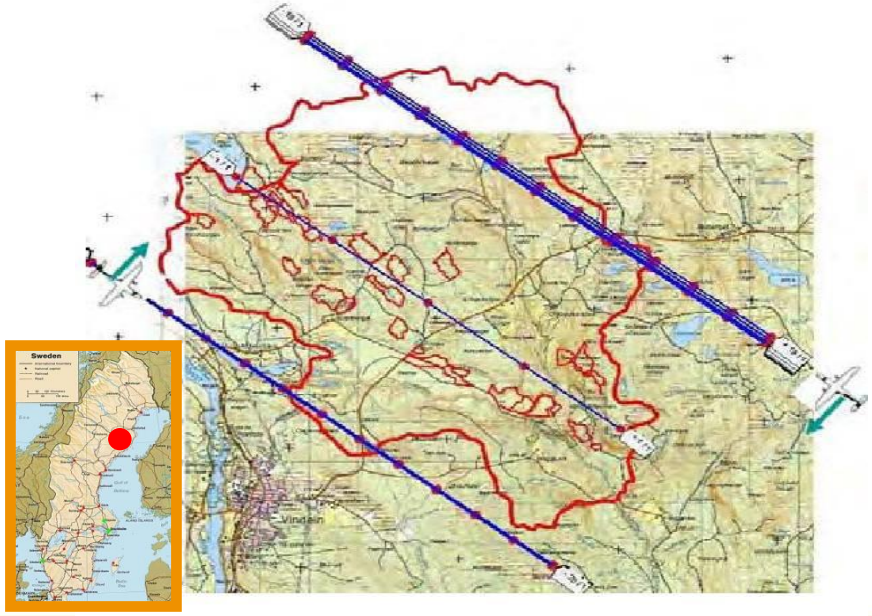

Tomographic Reconstruction of an azimuth cut:

Polarization: HV
Method: Capon Spectrum

Results are geocoded onto the same ground range, height grid

All panels have been re-interpolated such that the ground level corresponds to 0 m

Loss of resolution from near to far range, especially at P-Band ($\Delta z > 80$ m at far ranges)

Relevant contributions from the ground level below the forest are found at P-Band

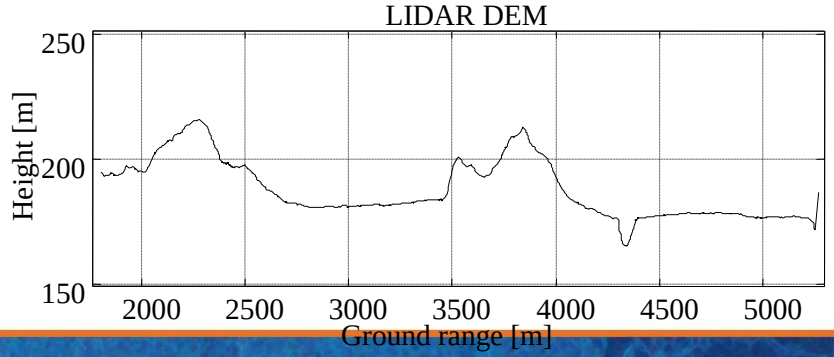

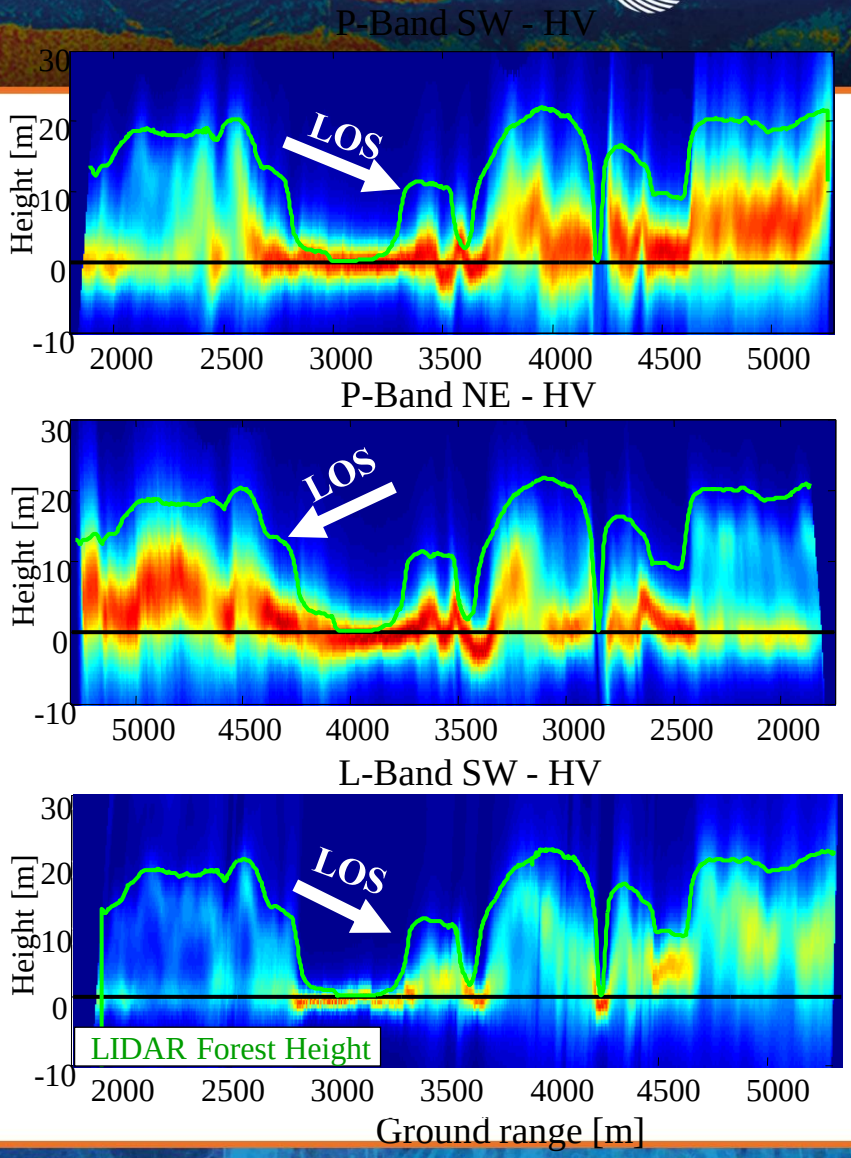

Model validation: $\mathbf{W} \overset{?}{=} \mathbf{C}_g \otimes \mathbf{R}_g + \mathbf{C}_v \otimes \mathbf{R}_v$

$$\hat{\mathbf{W}}_K = \arg\min_{\mathbf{W}_k} \left\{ \left\| \hat{\mathbf{W}} - \mathbf{W}_K \right\|_F \right\}$$

$$error = \frac{\left\| \hat{\mathbf{W}} - \mathbf{W}_K \right\|_F}{\left\| \hat{\mathbf{W}} \right\|_F}$$

Methodology:

evaluation of the error between the sample covariance matrix and its best L2 approximation with $K = \{1,2,3,4\}$ KPs

P-Band

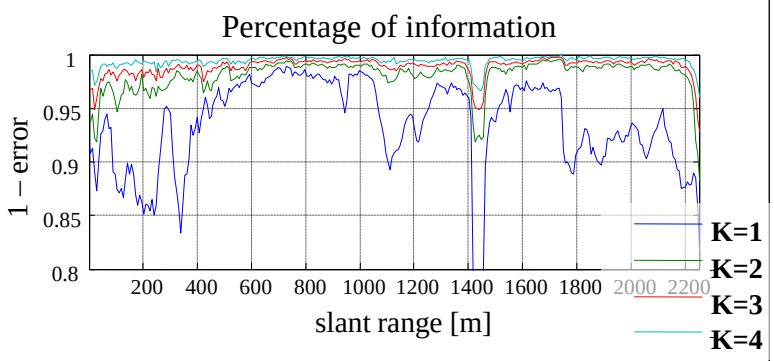

$$\left\| \hat{\mathbf{W}} - \hat{\mathbf{W}}_2 \right\|_F < 0.05 \cdot \left\| \hat{\mathbf{W}} \right\|_F$$

> 95 % of the information can be represented by the sum of just two KPs

L-Band

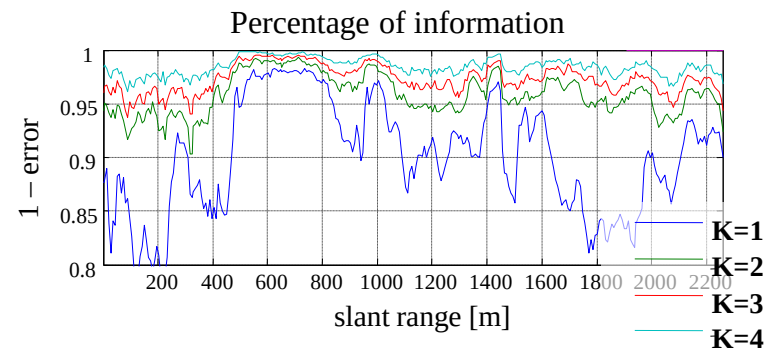

$$\left\| \hat{\mathbf{W}} - \hat{\mathbf{W}}_2 \right\|_F < 0.1 \cdot \left\| \hat{\mathbf{W}} \right\|_F$$

> 90 % of the information can be represented by the sum of just two KPs

Backscattered Power Distribution for Ground Scattering

Outer Boundary Solution

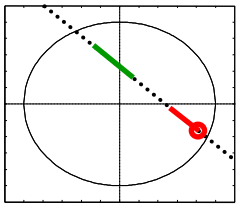

Significant rejection of volume contributions

Better results at P-Band, due to better ground visibility

Some leakage from the volume is present at L-Band in areas with dense forest and steep slopes

P-Band SW – Outer Boundary Solution

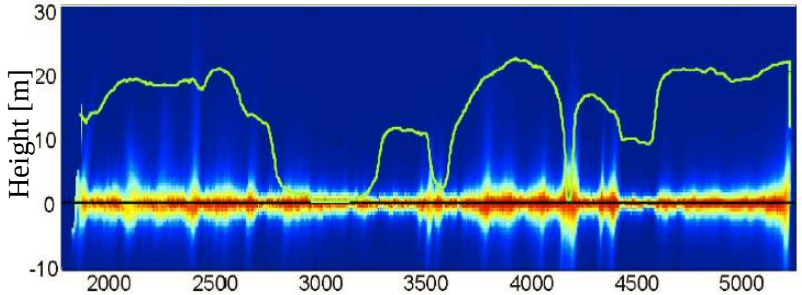

L-Band SW – Outer Boundary Solution

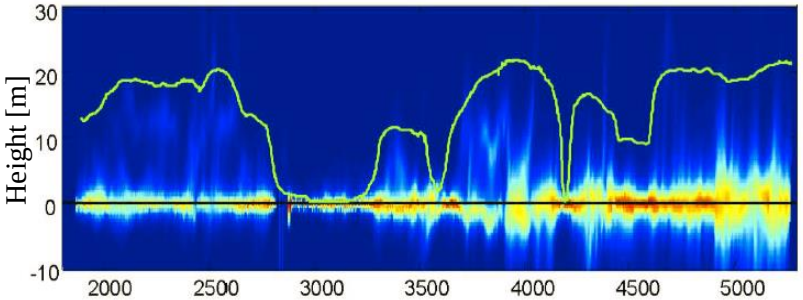

LIDAR DEM

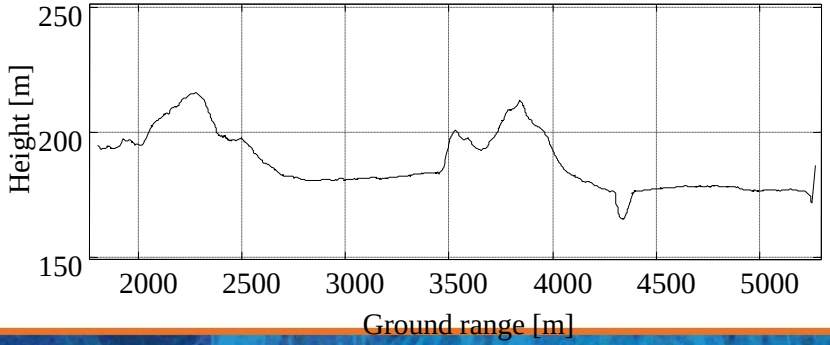

Backscattered Power Distribution for Volume Scattering

Inner Boundary Solution

$\mathbf{C}_g$ is singular

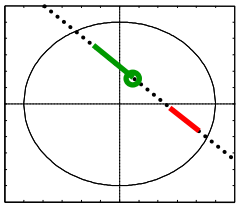

This solution corresponds to the polarization which is supposed not to be affected by ground contributions

P-Band

Significant contributions from the ground level.

⇔ Volumetric scattering at the ground level

Consistent with:

- Backscattering from understorey or lower tree branches
- Multiple interactions of volumetric scatterers with the ground

P-Band SW – Inner Boundary Solution

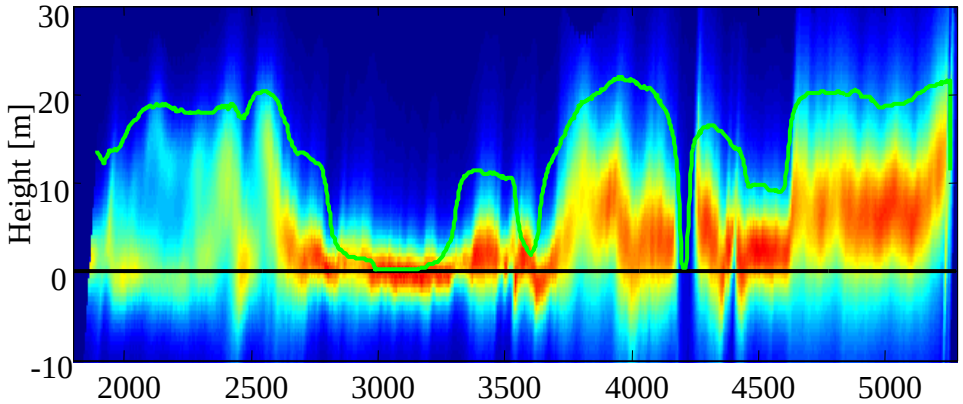

L-Band SW – Inner Boundary Solution

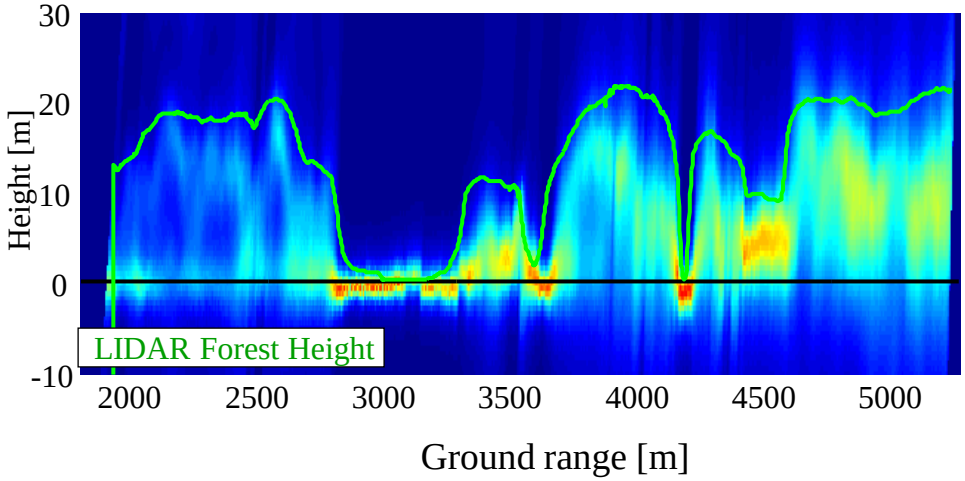

Backscattered Power Distribution for Volume Scattering

Intermediate Solution

$\mathbf{C}_g$ is full rank

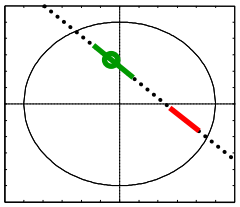

By moving from the inner to the outer boundary the contributions from the ground level are gradually rejected

P-Band

Backscattering contributions from the whole volume structure are emphasized

L-Band

Contributions from the lower canopy are partly rejected

Backscattering contributions from the upper volume structure are emphasized

P-Band SW – Intermediate Solution

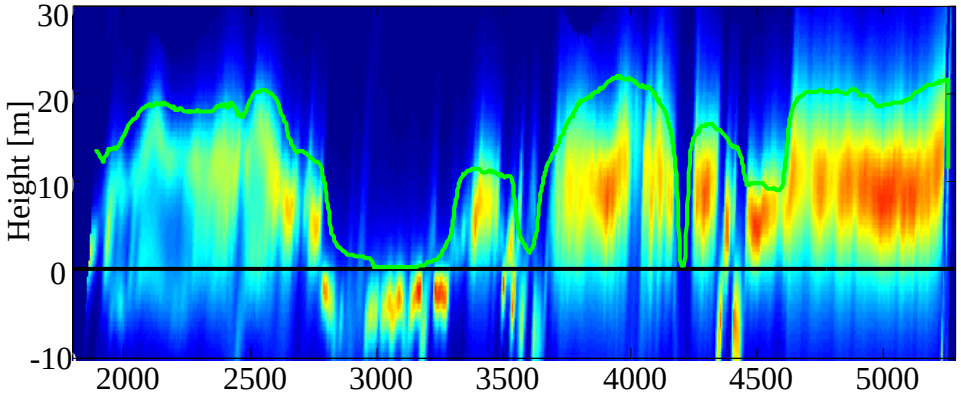

L-Band SW – Intermediate Solution

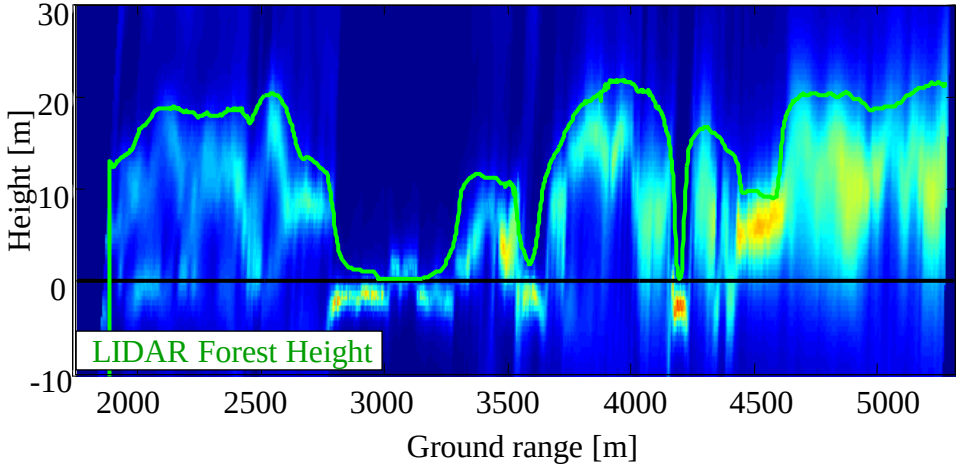

Backscattered Power Distribution for Volume Scattering

Outer Boundary Solution

$\mathbf{C}_g$ is full rank

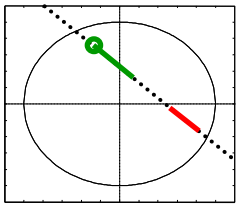

Only upper canopy contributions are visible, due to rejection of ground and lower canopy contributions

This phenomenon is more evident at P-Band, due to the coarse vertical resolution

Volume top height is nearly invariant to the choice of the solution, confirming the result of BioSAR 2007

P-Band SW – Outer Boundary Solution

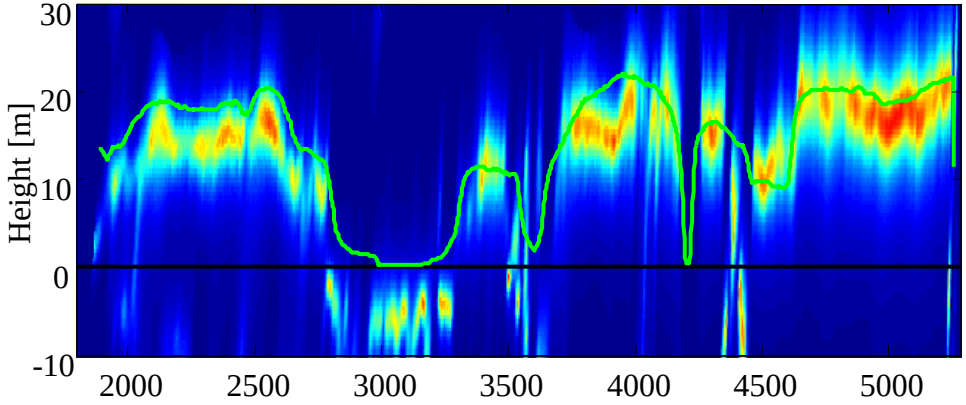

L-Band SW – Outer Boundary Solution

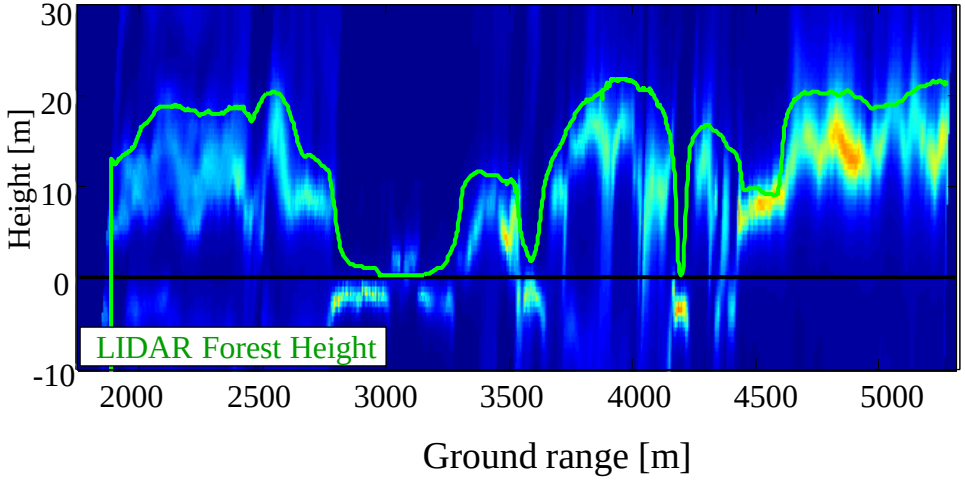

Campaign	TropiSAR- ESA
System	Sethi- ONERA
Period	August 2009
Site (among others)	Paracou, French Guyana
Scene	Tropical forest estimated 150 species per hectare Dominant families: Lecythidaceae, Leguminoseae, Chrysobalanaceae, Euphorbiaceae.
Tomographic tracks	6 – Fully Polarimetric
Carrier frequency	P-Band
Slant range resolution	≈1 m
Azimuth resolution	≈1 m
Vertical resolution	15 m

3D Imaging of the Guyaflux Tower

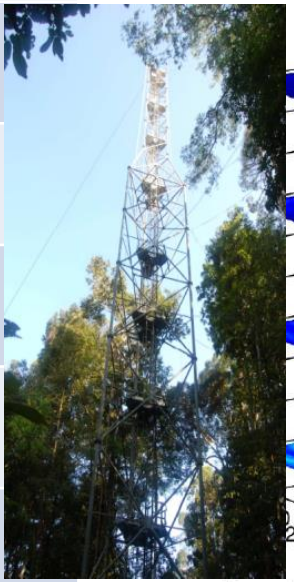

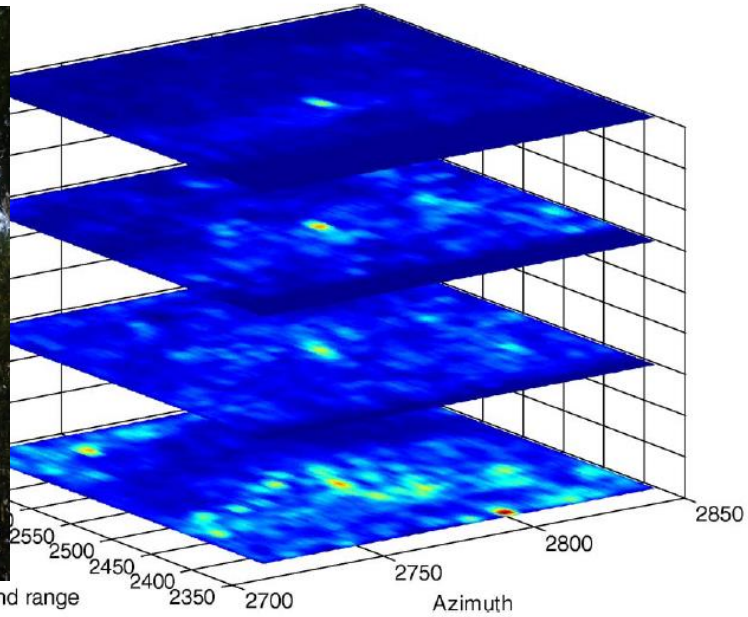

Tomographic Reconstruction of an azimuth cut:

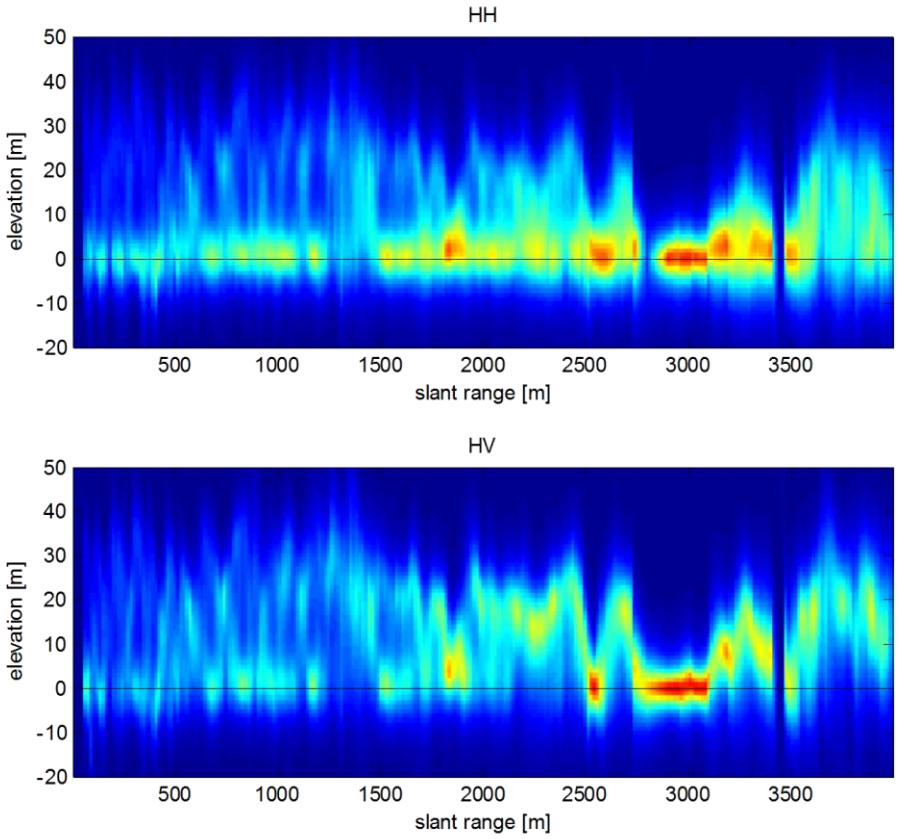

Visible contribution from the ground level beneath the forest

Vegetation is well visible

HV:
Poor contributions from the ground level beneath the forest

Vegetation is well visible

Model validation: $\mathbf{W} \overset{?}{=} \mathbf{C}_g \otimes \mathbf{R}_g + \mathbf{C}_v \otimes \mathbf{R}_v$

$$\hat{\mathbf{W}}_K = \arg\min_{\mathbf{W}_k} \left\{ \left\| \hat{\mathbf{W}} - \mathbf{W}_K \right\|_F \right\}$$

Methodology:

evaluation of the error between the sample covariance matrix and its best L2 approximation with $K = \{1,2,3,4\}$ KPs

$$error = \frac{\left\| \hat{\mathbf{W}} - \mathbf{W}_K \right\|_F}{\left\| \hat{\mathbf{W}} \right\|_F}$$

$$\left\| \hat{\mathbf{W}} - \hat{\mathbf{W}}_2 \right\|_F < 0.1 \cdot \left\| \hat{\mathbf{W}} \right\|_F$$

> 90 % of the information can be represented by the sum of just two KPs

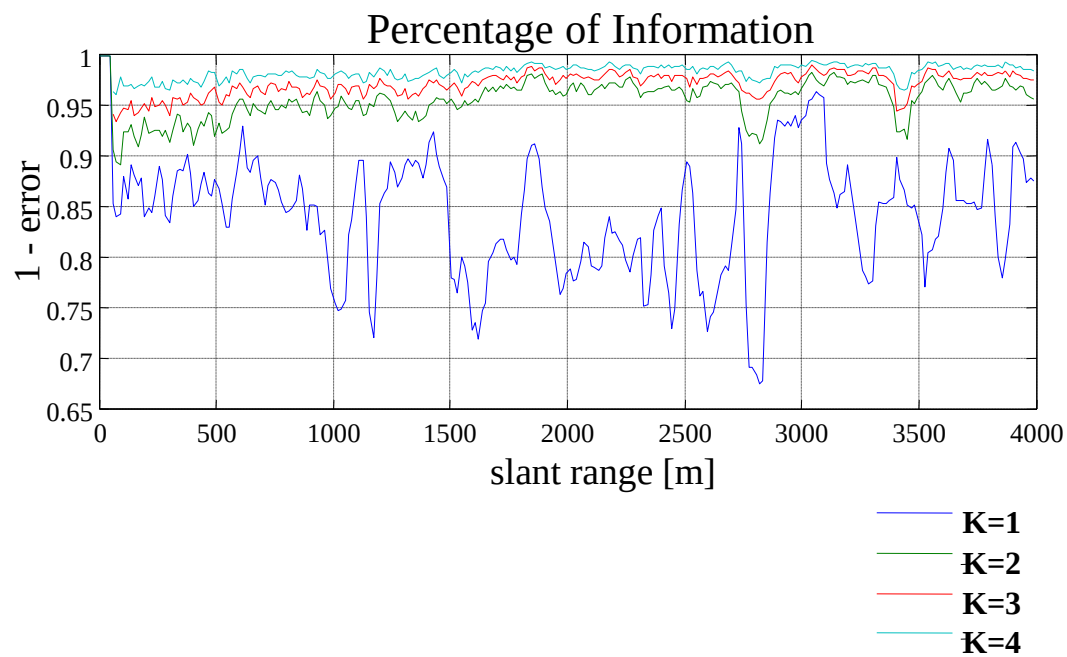

Inner boundary solutions

RPV

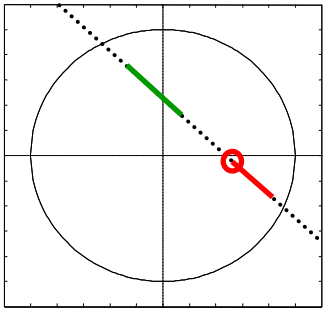

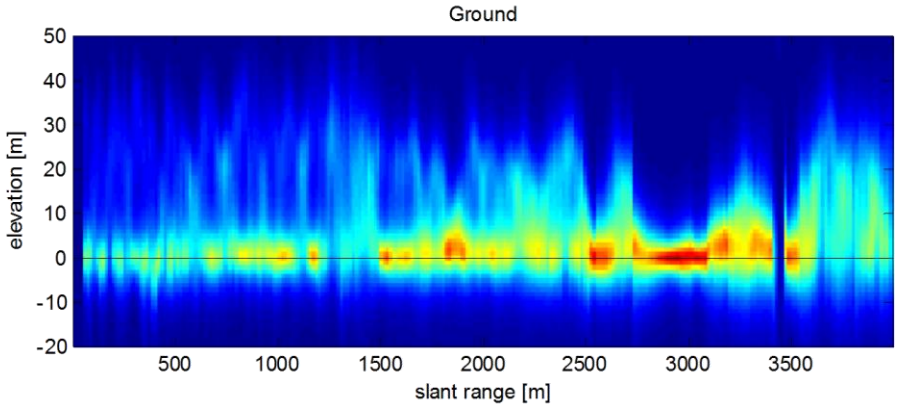

Strong volume contributions visible above the ground

Poor contributions from the ground level beneath the forest

Volume structure appears to be evenly distributed

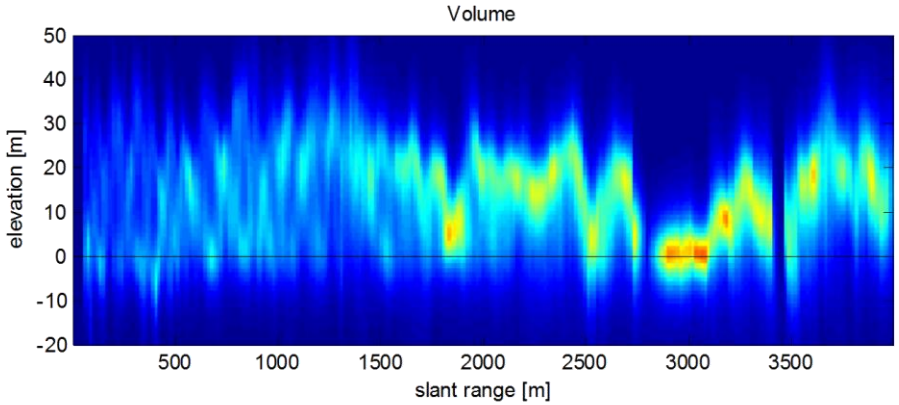

RPV

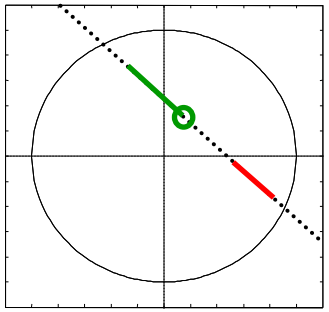

Intermediate solutions

RPV

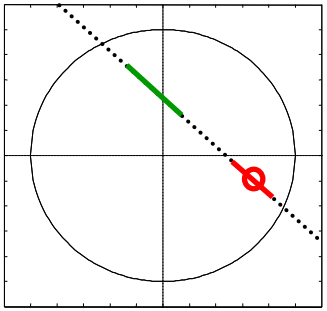

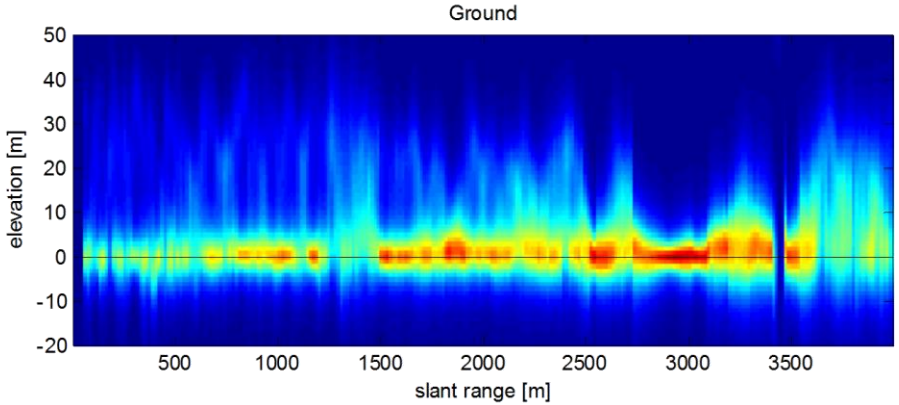

Improved volume rejection

Backscattering contributions from the upper volume structure are emphasized

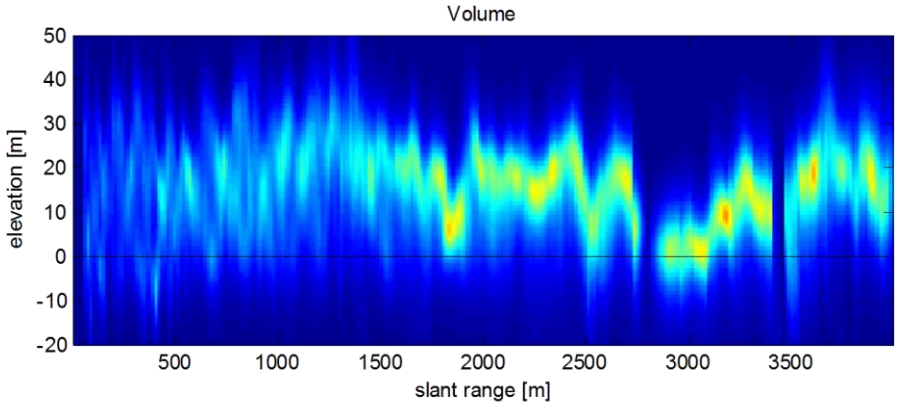

RPV

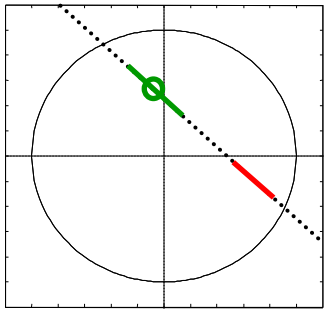

Outer boundary solutions

RPV

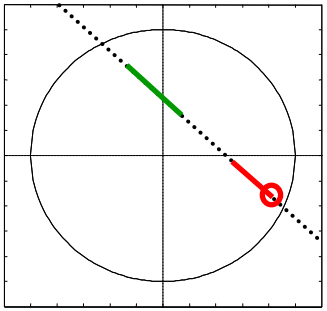

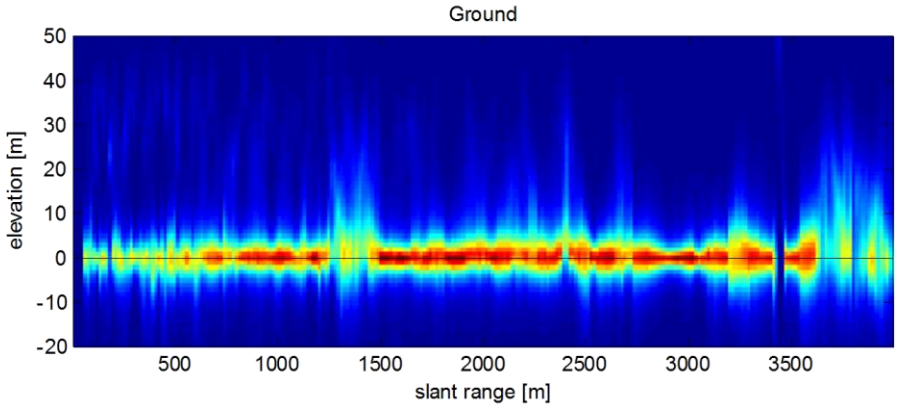

Maximum volume rejection

Ground structure is maximally coherent

Ground and lower canopy contributions are rejected

Only upper canopy contributions are visible

Volume structure is maximally coherent

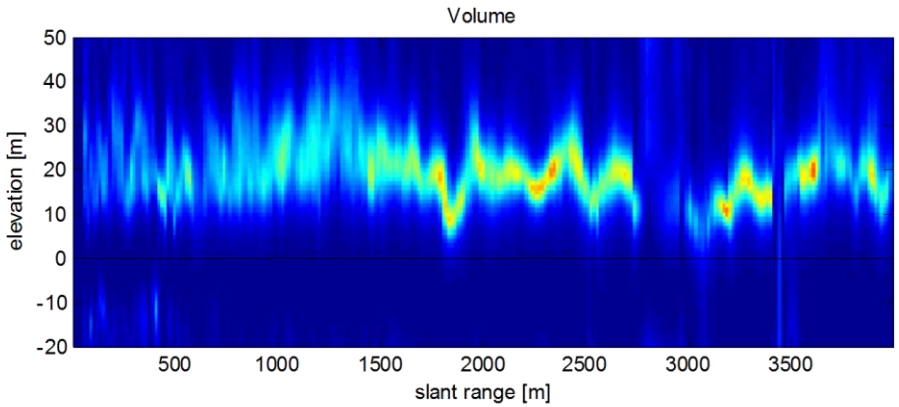

RPV

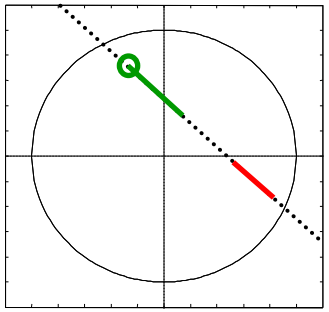

Volume top height is nearly invariant to the choice of the solution

References

Polarimetric and tomographic phenomenology of forests

- Reigber, A.; Moreira, A.; , "First demonstration of airborne SAR tomography using multibaseline L-band data," *Geoscience and Remote Sensing, IEEE Transactions on* , vol.38, no.5, pp.2142-2152, Sep 2000
- Mariotti d'Alessandro, M.; Tebaldini, S.; , "Phenomenology of P-Band Scattering From a Tropical Forest Through Three-Dimensional SAR Tomography," *Geoscience and Remote Sensing Letters, IEEE* , vol.9, no.3, pp.442-446, May 2012
- Frey, O.; Meier, E.; , "3-D Time-Domain SAR Imaging of a Forest Using Airborne Multibaseline Data at L- and P-Bands," *Geoscience and Remote Sensing, IEEE Transactions on* , vol.49, no.10, pp.3660-3664, Oct. 2011

Multi-layer optimization

- S. Sauer, L. Ferro-Famil, A. Reigber, E. Pottier, "Multi-aspect POL-InSAR 3D Urban Scene Reconstruction at L-Band", *Eusar 2008*
- Y. Huang, L. Ferro-Famil, A. Reigber, "Under Foliage Object Imaging Using SAR Tomography and Polarimetric Spectral Estimators", *Eusar 2010*

Coherence optimization

- M. Neumann, L. Ferro-Famil, A. Reigber, "Multibaseline Polarimetric SAR Interferometry Coherence Optimization", *IEEE Geoscience and Remote Sensing Letters*, 2008
- E. Colin, C. Titin-Schnaider, W. Tabbara, "An Interferometric Coherence Optimization Method in Radar Polarimetry for High-Resolution Imagery", *IEEE Transactions on Geoscience and Remote Sensing*, 2006

SKP decomposition: theory, algorithms and physical implications

- S. Tebaldini, "Algebraic Synthesis of Forest Scenarios from Multi-Baseline PolInSAR Data", *IEEE Transactions on Geoscience and Remote Sensing*, 2009
- Tebaldini, S.; Rocca, F.; , "Multibaseline Polarimetric SAR Tomography of a Boreal Forest at P- and L-Bands," *Geoscience and Remote Sensing, IEEE Transactions on* , vol.50, no.1, pp.232-246, Jan. 2012